Characterising the role of parametric functions in the van Genuchten empirical model on CO2 storage performance

Onoja, MU, Ahmadinia, M, Shariatipour, SM & Wood, AM

DOI 10.1016/j.ijggc.2019.06.004
ISSN 1750-5836

Publisher: Elsevier

Characterising the role of parametric functions in the Van Genuchten empirical model on CO_2 storage performance

Michael U. Onoja[a]*, Masoud Ahmadinia[a], Seyed M. Shariatipour[a], Adrian M. Wood[a]

[a]Centre for Fluid and Complex Systems, Maudslay House, Coventry University, Coventry, CV1 2NL, United Kingdom

*Corresponding author: onojau@coventry.ac.uk

Abstract

In the application of two-phase flow in porous media within the context of CO_2 sequestration, a non-wetting phase is used to displace a wetting phase residing *in-situ* to the maximum extent through a network of pore conduits. The storage performance of this physical process can be assessed through numerical simulations where transport properties are usually described using the Brooks & Corey (BC) or van Genuchten (vG) model. The empirical constant, namely the pore geometry index, is a primary parameter in both of these models and experimental evidence shows a variation in the value of this empirical constant. It is, therefore, essential to cast this empirical constant into a ternary diagram for all types of clastic porous media to demarcate the efficiency of two-phase flow processes in terms of the pore geometry index (PGI). In doing so, this approach can be used as a tool for designing more efficient processes, as well as for the normative characterisation of two-phase flow, taking into consideration the predominance of capillary pressure or relative permeability effects. This concept is based on the existence of a PGI estimation for clastic sediments, for which the value for 12 sediment mixtures fall between 1.01 and 3.00. Statistical data obtained from soil physics is used for developing and validating numerical models where a good match is observed in numerical simulations. In this context, a new methodology for the effective characterisation of PGI for different clastic rocks is proposed. This paper presents theoretical observations and continuum-scale numerical simulation results of a PGI characterisation for the prediction of the hydraulic properties of clastic reservoir rocks. The effect of key parameters in the vG empirical model, such as the pressure strength coefficient and the PGI, is incorporated into the simulation analysis. In particular, the model is used to investigate the effects of parameter representation on CO_2 storage performance in a saline aquifer. Subsequent analysis shows that the PGI is a very important parameter for defining the flow characteristics of simulation models. It can also be flexibly changed for each rock type and this approach may thus be practical when simulating the evolution of CO_2 plume in reservoirs with sedimentary heterogeneities, such as intra-aquifer aquitard layers or graded beds. The use of the realistic PGI boundaries promises a more precise description of the hydraulic behaviour in sandstones and shale when using either the BC or vG model.

Keywords: *CO_2 sequestration; Two-phase flow in porous media; Pore geometry index; Numerical simulation, Relative permeability; Capillary pressure*

1 Introduction

Reservoir modelling is a decisive tool for predicting CO_2 storage performance as it provides insight into the dominant processes of multi-phase fluid flow in a subsurface geologic media. It improves the understanding of fluid/rock interaction at different spatial and temporal scales, allowing accurate quantification of sequestration capacity and formation integrity, provided the geological data is not limiting. Sedimentary heterogeneities, primarily influenced by the geometry of depositional facies that control permeability structure, can be a limiting factor on characteristic hydraulic data of a storage unit. A scarcity of data on hydraulic properties, such as relative permeability [k_r] and capillary pressure [P_c] provide a challenge to dynamic flow modelling. Such scarcity is attributed to the site-specificity and tedious experimental validation of the k_r and P_c functions. Consequently, empirical models such as those proposed by Brooks and Corey (1964) and van Genuchten (1980) play an integral role in the description of k_r and P_c functions for geological formations. In view of the spatial variability factor associated with reservoir-scale investigations, these empirical models provide a viable means to characterise "capillary pressure - relative permeability - wetting saturation" (P_c – k_r – S_w) relations which aids in the accuracy of numerical solution to multi-phase fluid flow in porous media. Oostrom et al. (2016) conducted a comparative study on the performance of empirical models employed for CO_2 geo-storage and identified van Genuchten-Mualem-Corey (vG-MC) and Brooks-Corey-variable-Corey (BC-vC) models as the most suitable for $scCO_2$ injection simulations:

$$S_{ew} = \frac{S_w - S_{wr}}{S_{w,max} - S_{wr} - S_{nr}} \quad (1)$$

vG-MC:

$$P_c = P_g\left[(S_{ew})^{-1/m} - 1\right]^{1/n} \quad (2)$$

$$k_{rw} = (S_{ew})^{0.5}\left[1 - \left(1 - (S_{ew})^{1/m}\right)^{m}\right]^2 \quad (3)$$

$$k_{rn} = k_{rn}^0 \cdot (1 - S_{ew})^2(1 - S_{ew}^2) \quad (4)$$

BC-vC:

$$P_c = P_e\,(S_{ew})^{-\frac{1}{\lambda}} \quad (5)$$

$$k_{rw} = (S_{ew})^X \quad (6)$$

$$k_{rn} = k_{rn}^0 \cdot (1 - S_{ew})^2.[1 - (S_{ew})^Y] \quad (7)$$

where S_{ew} is the effective wetting saturation, S_w is the wetting saturation, and S_{wr} is the residual wetting saturation. The parameters, $S_{w,max}$ (the maximum wetting saturation) and S_{nr} (the residual non-wetting saturation) are determined by the flow dynamics. For the primary drainage (drying) curve, $S_{nr} = 0$ and $S_{w,max}$ is usually assumed as 1 for a wetting system, while for the primary imbibition (wetting) curve, $S_{nr} = S_{nr,max}$; and $S_{w,max} \neq 1$. P_e is the capillary entry pressure, k_{rn}^0 is the end-point relative permeability to the non-wetting phase, and P_g is the strength coefficient expressed as the inverse of the pressure scaling parameter, α. The

variables, λ, n, and m are fitting parameters known as the pore size/geometry index while X and Y are known as Corey exponents for the wetting and non-wetting phase, respectively.

Justifications for the wide utilisation of these geometry-based empirical models include the relative ease of their implementation in numerical simulators in the absence of site-specific $P_c - k_r - S_w$ data, as well as the relative fit of experimentally determined $P_c - k_r - S_w$ curves to the BC-vC model through λ, X and Y e.g. Perrin and Benson (2010), Bachu (2013), and Krevor et al. (2012). The use of the BC-vC rather than vG-MC for this purpose is mainly due to the inclusion on the capillary entry pressure in the former. Nevertheless, the latter approach has been increasingly adopted in the numerical modelling of subsurface $scCO_2$ and brine transport during the last decade (Birkholzer et al., 2015; Doughty, 2010; Liu et al., 2011; Middleton et al., 2012; Okwen et al., 2011; Pruess and Nordbotten, 2011; Yamamoto and Doughty, 2011; Zhou et al., 2010). Most of these studies, however, utilised the van Genuchten model within simplified parametric descriptions of the pore geometry index [n] and the strength coefficient [P_g], which may require revising. The first important consideration is the description of n [where $n = 1/(1-m)$], which usually includes a generic value of $n \approx 2.0$ for sandstone aquifer and even shale aquitard (see Birkholzer et al., 2009; Espinet et al., 2013; and Gor et al., 2013). This assumption may not be ideal practice in geological CO_2 sequestration (GCS) since the variability in the pore size index normally provides a reasonable fit to available experimental data (Doughty et al., 2008). Secondly, the strength coefficient P_g (where $P_g = 1/\alpha$) in the vG-MC model has been referred to as the capillary entry pressure [P_e] in studies by Zhou et al. (2008) and Mathias et al. (2013). This is inconsistent with van Genuchten's (1980) description of the pressure scaling parameter at the maximum pore throat radius [R_{max}] which is larger than the capillary entry pressure i.e. $\alpha P_e < 1$. According to van Genuchten (1980), an inflection point on the capillary pressure curve is usually required in order to determine the value for the model's pressure scaling parameter [α]. Hence an assumption of $\alpha P_e = 1$ usually results in a wide discrepancy between the BC's and vG's description of the flow model. Nevertheless, the introduction of capillary entry pressure is generally advisable when using the Mualem model (as is the case with vG-MC) irrespective of the parameter function used to describe the effective wetting saturation (Ippisch et al., 2006). The crucial point in applying Mualem's model is the correct evaluation of the integral:

$$\int_0^{S_{ew}} \frac{1}{P_c(S_w)}\, dS_w = -\int_{P_c(S_{ew})}^{\infty} \frac{1}{P_c(S_w)} \cdot \frac{dS}{dP_c} \cdot dP_c \qquad (8)$$

If a capillary entry pressure value is not introduced in the parameterisation of the capillary pressure curve then a decrease in the absolute value of the derivative of the capillary pressure curve $|\frac{dS}{dP_c}|$ must be faster than the increase of $\frac{1}{P_c}$ for $P_c \to 0$. These conditions are general and independent of the specific model used for the capillary pressure curve. Thus, the absence of

the capillary entry pressure in the vG model imposes a constraint of $n \geq 1.88$ when it is coupled to the Mualem model (Fuentes et al., 1992). However, fine-textured sediments may exhibit n-values in the range of $1 < n < 2$ (e.g. Carsel and Parrish, 1988), therefore, the introduction of a capillary entry pressure in the vG model is obligatory if $n < 2$ (Ippisch et al., 2006). It becomes advisable to introduce some sort of parameter equivalence between the van Genutchten and Brooks-Corey equations when describing the hydraulic properties of sedimentary formations using vG model. This helps to quantify the capillary entry pressure during vG computations.

To the best of our knowledge, no numerical study has been conducted to determine whether the constancy of the pore geometry parameter in a field introduces a bias in the predicted CO_2 storage performance. Besides, little information exists on the effect of using different values for n to represent different rock lithologies in a reservoir/seal system. To begin addressing these issues this study applies linear parameter estimation techniques to fit vG's pore geometry parameter [n] in soil hydraulic behaviour to the rock hydraulic behaviour. This approach is implemented by comparing the different heterogeneous pore systems of sand and clay and their consolidated counterparts, sandstone and claystone, assuming the same level of consolidation, no cementation, and the percentage composition of clastic sediments are approximal in both porous media. This should avoid discrepancies in the systematic behaviour of predicted relative permeabilities in soils and rocks. Of particular interest is information on improving the predicted values of relative permeability that do not require prolonged experimental measurements for validation purposes. Rather than focus on all sedimentary rock types that are suitable for GCS, this paper only highlights siliciclastic rocks which have defined grain-size categories. Once estimated, the optimised model parameters will be used to investigate the relationships between sedimentary heterogeneities in siliciclastic rocks and CO_2 storage performance in aquifers. Since the $P_c - k_r - S_w$ relationship is expressed in the form of analytical functions facilitating their inclusion into numerical simulation models, it should enable a rapid comparison of the hydraulic properties of different siliciclastic rocks.

The specific purpose of this study is to characterise the pore geometry index of the vG-MC model to siliciclastic rock formations. This study adopts a of clastic rock classification based on particle size and chosen sediment structures (Potter et al., 1980; Stow, 1981). Herein, principles and methods used in soil mechanics are applied, utilising a limited set of predictors that focus mainly on grain size distribution. The contribution of other effects such as the wettability of the porous medium, fluid viscosity and the interfacial tension between the fluids in contact is not considered in the parameterisation scheme.

2 Description of pore geometry index, *n*, in vG model for siliciclastic rocks

Volumetrically, siliciclastic rocks are the dominant sedimentary formations for GCS (Boggs, 2009). To describe the pore geometry index in van Genuchten model for clastic rocks, it is important to first define such rocks. Clasts or rock fragments vary in size from fine clay and silt, through sand, to coarse-grained pebble, cobble and boulder. Sand clasts are defined by the United States Department of Agriculture (USDA, 1987) and the British Standards Institution (BSI, 1990) as having a diameter from 0.06 to 2.00 mm. Silt clasts are 0.06 to 0.002 mm, while clay is ≤ 0.002 mm. Using the Wentworth (1922) Scale, the terms very coarse sandstone, coarse sandstone, medium sandstone, fine sandstone, and very fine sandstone are used for psammites (Table 1). However, some fine-grained sedimentary rocks are not as precisely defined, while the classification of shale is more ambiguous (Flemming, 2000; Macquaker and Adams, 2003; Picard, 1971; Potter et al., 2005). Shale has been regarded as mudrocks that show fissility, i.e. a strong tendency to split or break (Ingram, 1953). Mudrocks exhibit a much wider grain size distribution than sandstones, with grain diameters typically ranging over three orders of magnitude, and include both silts and clays (Aplin et al., 1999; Dewhurst et al., 1998).

<table>
<tr><th>Geological size (mm)</th><th>Sediment Texture</th><th colspan="2">General term for Consolidated Rock</th></tr>
<tr><td>2.0 - 1.0</td><td>Very coarse sand</td><td colspan="2" rowspan="5">Sandstone</td></tr>
<tr><td>1.0 - 0.5</td><td>Coarse sand</td></tr>
<tr><td>0.5 - 0.25</td><td>Medium sand</td></tr>
<tr><td>0.25 - 0.125</td><td>Fine sand</td></tr>
<tr><td>0.125 - 0.0625</td><td>Very fine sand</td></tr>
<tr><td>0.0625 - 0.0313</td><td>Coarse silt</td><td rowspan="4">Siltstone</td><td rowspan="5">Mudrock (Shale)</td></tr>
<tr><td>0.0313 - 0.0156</td><td>Medium silt</td></tr>
<tr><td>0.0156 - 0.0078</td><td>Fine silt</td></tr>
<tr><td>0.0078 - 0.0039</td><td>Very fine silt</td></tr>
<tr><td>< 0.0039</td><td>Clay</td><td>Claystone</td></tr>
</table>

Table 1: The Wentworth scale for clastic sediments (Wentworth, 1922)

Siliciclastic rocks can be classified using the soil textural triangle developed by the US Department of Agriculture (USDA, 1987) and the recommended ternary diagram for naming clasts (Shepard, 1954) as shown in Fig. 1. This classification scheme can be further sub-divided into muddy sand and sandy mud (Fig. 2) and is used to define siliciclastic rocks (Table 2).

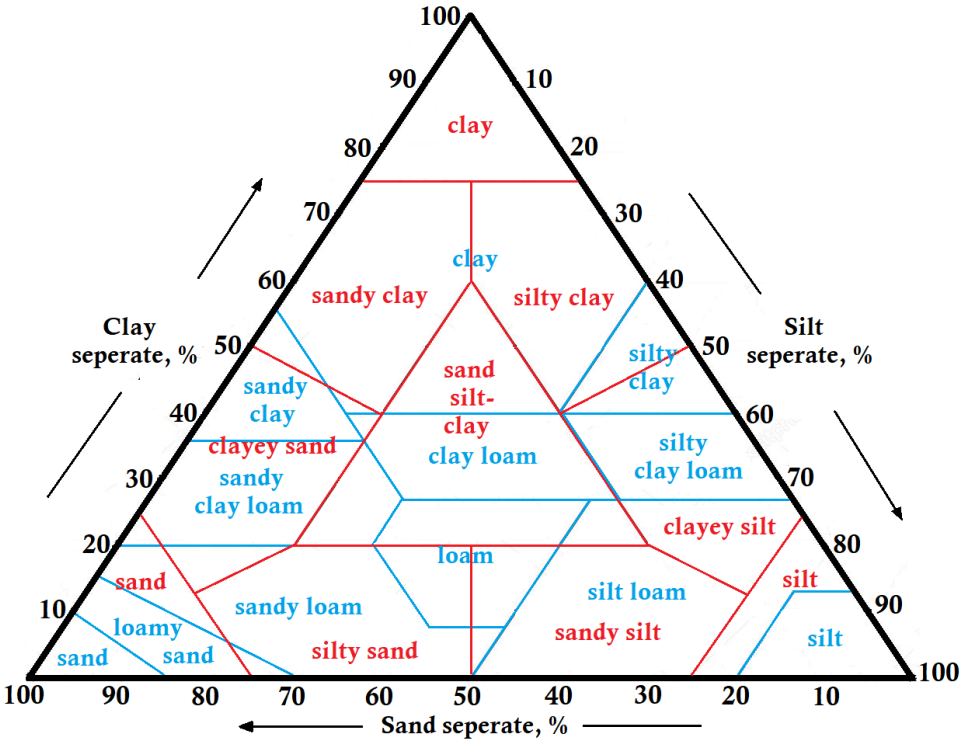

Fig. 1: Correlation between USDA (1987) soil texture triangle and recommended conceptual scheme for the nomenclature of mixed clastic sediments. *NB: See Appendix A, Fig A1 for seperate triangles.*

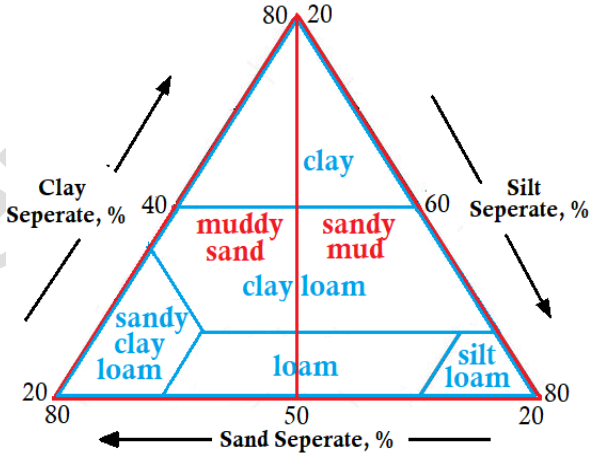

Fig. 2: Sub-division of the sand silt-clay triangle in Fig. 1

Recommended nomenclature for clastic sediments (from Shepard 1954)	*Equivalent textural classification (from USDA 1987)*	*Sedimentary composition (adopted from USDA 1987)*			*Proposed terminology for clastic rock in this study*	*General term for sedimentary rock in literature*
		% Sand	*% Silt*	*% Clay*		
Sand	Sand	≥ 85	Silt + 1.5Clay ≤ 15		Coarse-textured Sandstone	Sandstone

	Loamy Sand	70 - 85	Silt + 2Clay ≤ 30		Medium-textured Sandstone	
Silty Sand	Sandy Loam	≥ 50	Silt + 2Clay > 30	≤ 20	Fine-textured or Silty Sandstone	Sandstone
Clayey Sand	Sandy Clay Loam	≥ 45	< 28	20 - 35	Very Fine-textured or Clayey Sandstone	Sandstone
Sandy Silt	Silt Loam		≥ 50	< 27	Coarse-textured or Sandy Siltstone	Sandstone
Silt	Silt		≥ 80	< 12	Siltstone	Mudrock
Clayey Silt	Silty Clay Loam	< 20		27 ≤ Clay ≥ 40	Clayey Siltstone or Silty Mudstone	Mudrock
Muddy Sand*	Sandy Clay Loam + Loam + Clay Loam + Clay	≥ 50*	Clay + 2Silt ≥ 40*		Muddy Sandstone*	Sandstone
Sandy Mud*	Silt Loam + Loam + Clay Loam + Clay	20 – 45*	Clay + Silt ≥ 40*		Mudstone*	Mudrock
Sandy Clay	Sandy Clay	≥ 45		≥ 35	Sandy Claystone	Mudrock
Silty Clay	Silty Clay		≥ 40	≥ 40	Silty Claystone	Mudrock
Clay	Clay	< 45	< 40	≥ 40	Claystone	Mudrock
**Nomenclature and sedimentary composition suggested in this study*						

Table 2: Naming convention proposed for siliciclastic rocks

Carsel and Parrish (1988) estimated, through statistical analysis of a sample size between 46 and 1183, the spatial representation of van Genuchten's (1980) pore geometry parameter [*n*] in all twelve of the USDA's soil textural classes. The application of this data provides a basis upon which associated pore geometry index for the siliciclastic rocks, as defined in Table 2 are referred to in this study. Estimated vG n-values are extapolated for the siliciclastic rocks and shown in Table 3. This is based on the applicability of the van Genuchten model in both soil and rock mechanics. Fundamental to this approach, however, is the need to establish good approximations to empirical distributions for n-values for each siliciclastic rock in Table 3. In this regard, a senstivity analysis on *n*-values ranging from 1.01 to 3.00 is described in Section 4.

Siliciclastic rock	*Pore-geometry parameter, n (from Carsel and Parrish, 1988)*	*Textural classification adopted for siliclastic rocks in this study*
Coarse Sandstone	2.68	Very coarse
Sandstone	2.28	
Silty Sandstone	1.89	Coarse
Muddy Sandstone	1.56	
Clayey Sandstone	1.48	
Sandy Siltstone	1.41	Medium
Siltstone	1.37	
Mudstone	1.31	
Clayey Siltstone or Silty Mudstone	1.23	Fine
Sandy Claystone	1.23	
Silty Claystone	1.09	Very fine
Claystone	1.09	

Table 3: Descriptive *n*-values in van Genuchten model for clastic rocks

3 Parameter equivalence between BC and vG models

In the vG P_c model (Eqn. 2), the pressure scaling parameter, α (where $\alpha = 1/P_g$) the pore geometry index, n, the maximum wetting saturation, $S_{w,max}$, and the residual wetting saturation, S_{wr}, are independent parameters that can be estimated from experimental P_c – S_w *data*. It is convenient to express $S_{w,max} = 1$ and assume that S_{wr} (the water content where S_{ew} equals zero) is a well-defined parameter in GCS of water-wet systems. Theoretical descriptions of α in literature are usually through a parameter equivalence between BC and vG, which describes an empirical relationship between the capillary entry pressure [P_e] in BC models and the pressure-scaling parameter [α] in vG models. Van Genuchten (1980) suggested that for large capillary pressure values, which will be the case in fine-textured sediments, the classical vG model reduces to the BC model where $\lambda = mn$. In an attempt to account for all sediment textures, i.e. from coarse to fine grained, Ippisch et al. (2006) modified the van Genutchen model to directly incorporate a capillary entry pressure value by introducing a parameter, S_c (where S_c, the saturation at cut-off point, = $[1 + (\alpha Pe)^n]^{-m}$]) but this term is restricted to fluid models where $\alpha P_e \gg 1$. Vogel and Cislerova's (1988) proposition for deriving a van Genuchten model including a capillary entry pressure introduced an arbitrary parameter, S_m (where $S_m \geq S_{w,max}$). However, this arbitrary parameter makes the author's theorem unsuitable in describing completely water wet systems and should only be considered as an additional fitting parameter that may enable a more precise description of k_r and P_c functions near saturation, especially for $n < 2$ (Vogel et al., 2000). Li et al. (2013) described a vG-type P_c model (Eqn. 9) with the

inclusion of a "threshold" non-wetting phase saturation, S_{nt}, which defines the width of the entry-slope region in the vG model (Fig. 3).

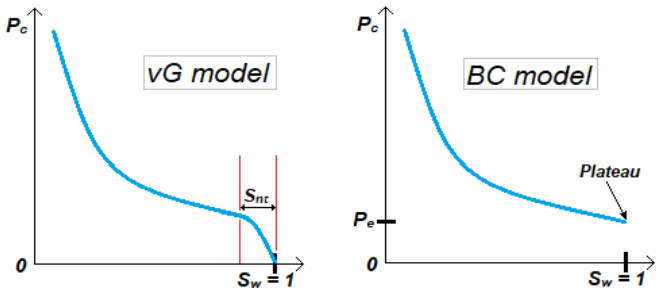

Fig. 3: Description of P_c – S_w curves for vG and BC analytical models

$$P_c = P_e\left(\frac{S_w - S_{wr}}{1 - S_{wr}}\right)^{-\frac{1}{\lambda}} \qquad \text{if } S_{wr} \le S_w \le 1 - S_{nt} \qquad (9a)$$

$$P_c = \frac{P_e}{S_{nt}}\left(\frac{1 - S_{nt} - S_{wr}}{1 - S_{wr}}\right)^{-\frac{1}{\lambda}}(1 - S_w) \qquad \text{if } 1 - S_{nt} < S_w \le 1 \qquad (9b)$$

Eqn. 9, however, does not reflect the original van Genuchten model and is theoretically a replica of the BC model where an exception is made for the capillary pressure at a wetting saturation of unity to be equivalent to zero, i.e. $P_{c(Swr=1)} = 0$. Morel-Seytoux et al. (1996) suggested a parameter equivalence between Brooks-Corey and van Genuchten by introducing the following mathematical expressions for coupled Mualem formulations (Eqn. 10). Its applicability is, however, limited as it is based on a fully defined value for the pore scaling parameter [α] and fails to identify a relationship between the pore size index of Brooks-Corey model, λ and van Genuchten model, n.

$$P_e = \left(\frac{1}{\alpha}\right)\frac{(p+3)}{2p(p-1)}\left(\frac{147 + 8.1p + 0.092p^2}{55.6 + 7.4p + p^2}\right) \qquad \text{where } p = 1 + (2/m). \qquad (10)$$

Lenhard et al. (1989) identified this relationship in the authors' mathematical expressions for parameter equivalence between Brooks-Corey and van Genuchten for $P_c > P_e$:

$$\lambda = \frac{m}{1-m}\left(1 - Z^{\frac{1}{m}}\right) \qquad (11)$$

where Z represents the match-point effective wetting saturation, i.e. midway between the saturated wetting fluid saturation and irreducible saturation, and equals 0.5. In this study, Eqn. 11 agrees with van Genuchten's (1980) summation that λ is equivalent to the product of m and n for fine-textured sediments. This is seen in Table 3 for λ-values of fine and very fine siliciclastic rocks, correct to one decimal place. Therefore, the parameter equivalence for BC and vG employed herein is described by:

$$\alpha = \frac{(S_{ew})^{\frac{1}{\lambda}}}{P_e} \cdot \left[(S_{ew})^{-1/m} - 1\right]^{1-m} \qquad (12)$$

where λ is computed from Eqn. 11.

4 Pore Geometry Index, *n*, sensitivity study for CO_2 geo-sequestration

A sensitivity analysis is presented here to distinguish between the values for *n* (i.e. *n*-values) that have the same significance on *in-situ* CO_2 plume shape and overall assessment of CO_2 geo-storage. Using the vG-MC model, hysteretic $P_c - k_r - S_w$ curves are computed for *n*-values ranging from 1.01 to 3.00, with an increment of 0.01, to account for each value of *n* listed in Table 3. The approach taken in this study requires a realistic characterisation of parameter uncertainty, therefore, the residual wetting saturation [S_{wr}] is held constant for all values of *n*. This indicates a constant relative permeability to the non-wetting phase [k_{rCO2}] in the sensitivity study thus accounting for the role of the pore geometry index in CO_2 storage performance. To make the sensitivity analysis computationally tractable, the system model assumes a 200m-thick isotropic saline aquifer with axisymmetric geometry of 1km in radial length and an incompressible siliciclastic rock with homogeneous rock properties. The reservoir is initially fully saturated with brine and no-flow conditions are assumed across the lateral and vertical boundaries of the domain. A black oil simulator, ECLIPSE 100 (E100), is used to simulate the injection of supercritical CO_2 (scCO2) through a single injection well into the reservoir under isothermal conditions. The well is situated at the leftmost boundary (r = 0), perforated across the bottom half of the permeable reservoir, and $scCO_2$ is injected for 10 years at a constant rate of 0.3 Mt/year. The radius of the domain and injection rate of CO_2 are chosen so that the gas saturation front is far from the boundary and there is negligible effect of these parameters on the motion of the saturation front during the injection period. Irreducible CO_2 saturation for drainage and imbibition are assumed to be 0 and 0.412, respectively. Other parameters used in the simulation are summarised in Table 4.

Parameter	*Value*
Porosity	0.14
Permeability	50 mD
Initial pressure	10,000 KPa
Temperature	33°C
Brine salinity	300,000 ppm
Capillary entry pressure	1.622 KPa
Maximum brine saturation	1.0
Residual brine saturation	0.3
End-point relative permeability to brine	1.0
End-point relative permeability to CO_2	0.623

Table 4: Parameters used for the E100 simulations

In accounting for both parameter uncertainty and the role of the parameter [*n*] in the model, *n*-values are ranked based on four criteria: (i) the shape of the plume, (ii) the maximum radial extension of the plume at the base of the reservoir model, (iii), the mobile gas fraction, and

(iv) the percentage volume of residual CO_2 saturation, at the end of $scCO_2$ injection. This is described in Section 4.1. Although residual trapping mostly occurs after CO_2 injection stops owing to flow reversal where the wetting fluid imbibes into the CO_2 plume. However, residual saturation can also occur during CO_2 injection and this can be calculated when imbibition curves are introduced in the forward modelling exercise. At the onset of CO_2 injection, the movement of CO_2 plume as a gravity current in the reservoir will gradually lead to up-dip deceleration and subsequent isolation and immobilization of CO_2 bubbles in pore spaces. This isolation is regarded, in literature, as "snap-off" of CO_2 plume in the trailing edge. Dullien (1991) attributed this "snap-off" to wettability and capillary effects in the porous media.

4.1 Parameter sensitivity analysis

A MATLAB code coupled to ECLIPSE (see Appendix A, Algorithm A1) was employed to compute $P_c - k_r - S_w$ relations, using the vG model, and generate 200 realisations for reservoir simulation using the pore geometry spectrum ***n=1.10:0.01:3.00*** (i.e. n varies from 1.10 to 3.00 with incremental intervals of 0.01). Numerical simulations of CO_2 injection for $1.01 \leq n \leq 1.09$ were truncated due to the extremely steep $P_c - S_w$ curve for these n-values, thus hindering CO_2 injection in the domain. Nevertheless, CO_2 injection was initiated for all other n-values and the simulation results of injected CO_2 with time showed a linear and constant relationship for all n-values. This culminated in a total injected CO_2 of 3Mt in each sensitivity case for $1.10 \leq n \leq 3.00$ at the end of simulation. This was expected since the total injected CO_2 is highly sensitive to the end-point relative permeability to CO_2 (Yoshida et al., 2016), which was held constant for all n-values in the study. Table 5 and Fig. 4 illustrate the sensitivity to n-values according to criteria III and IV, respectively. It can be seen that the ranking of the pore geometry index is consistent with descriptive values in Table 3. Values in Fig. 4 are characterised based on a 0.3 percentage increase for very coarse-, coarse- and medium-textured siliciclastic rocks, and a 1- and 2-percentage increase for fine and very-fine textured siliciclastic rocks, respectively (see Table 3). This is based on inductive inference from failed simulation runs for n-values between 1.01 and 1.09, suggesting that the alignment of n-values situated at the lower end of the spectrum, ***n=1.10:0.01:3.00***, results in a steeper curve for the illustration of the computed residual CO_2 saturation described in Fig. 4. Table 5, which shows the average range with an increment value of 6×10^{-5} for mobile CO_2 saturation in the domain, supports this approach and validates the distribution of n-values obtained from Carsel and Parrish (1988) for various siliciclastic rocks in Table 3.

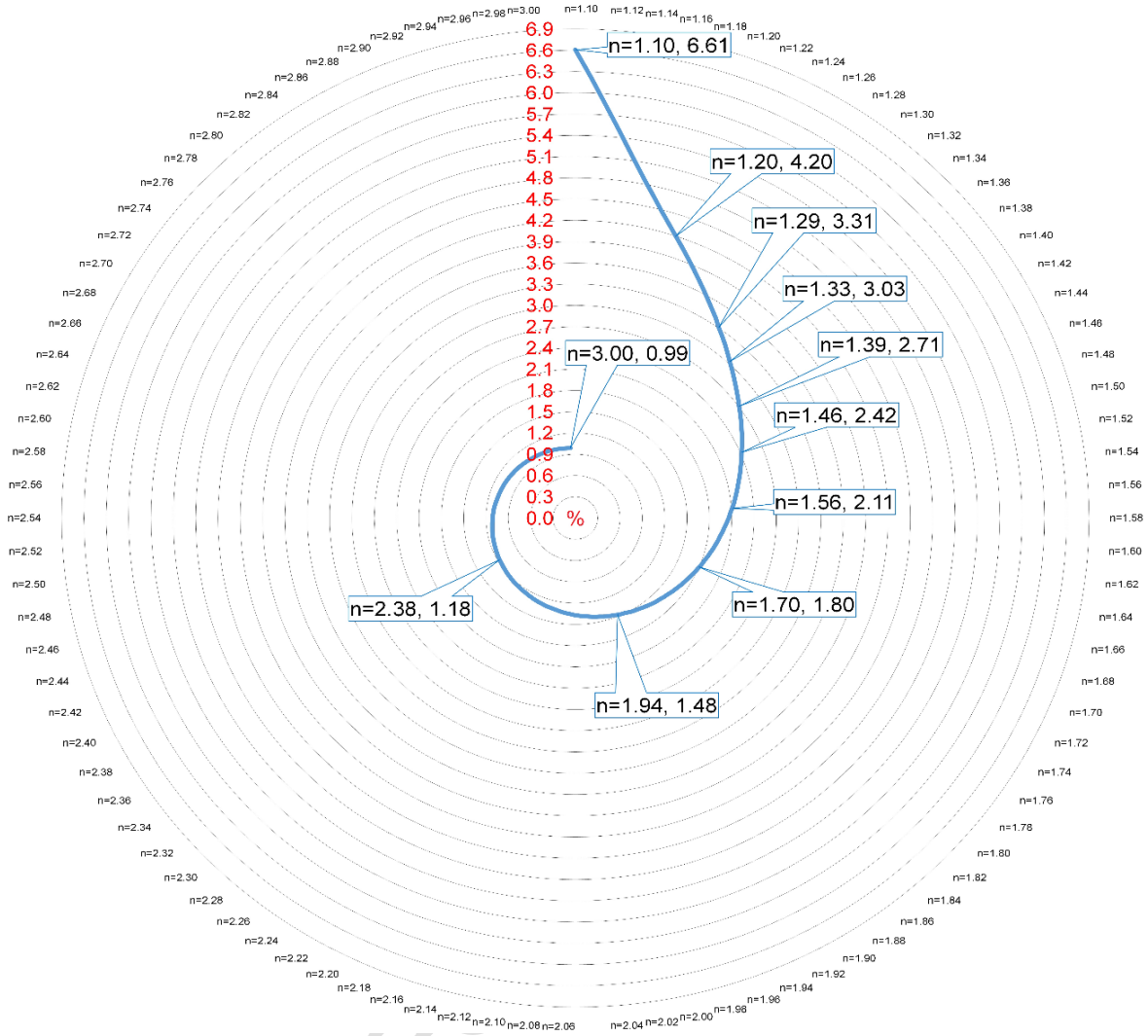

Fig. 4: Percentage volume of residual CO_2 at the end of simulation. NB: Data outcalls show the value for *n* and correponding percentage of residual CO_2 saturation while the *n*-values outside the ring indicate the range of values analysed.

Average field gas saturation range	*Pore geometry index, n*	*Siliciclastic rock*
0.02664 – 0.02655	3.00 – 2.37	Coarse sandstone
0.02654 – 0.02645	2.36 – 1.93	Sandstone
0.02644 – 0.02635	1.92 – 1.70	Silty Sandstone
0.02634 – 0.02625	1.69 – 1.56	Muddy Sandstone
0.02624 – 0.02615	1.55 – 1.45	Clayey Sandstone
0.02614 – 0.02605	1.44 – 1.38	Sandy Siltstone
0.02604 – 0.02595	1.37 – 1.32	Siltstone
0.02594 – 0.02585	1.31 – 1.28	Mudstone
0.02584 – 0.02575	1.27 – 1.24	Silty Mudstone
0.02574 – 0.02565	1.23 – 1.21	Sandy Claystone
0.02564 – 0.02555	1.20 – 1.19	Silty Claystone
0.02554 – 0.02500	1.18 – 1.10	Claystone

Table 5: Characterisation of the average gas stauration range to the pore geometry parameter range

Fig. 5 depicts the effective saturation distribution for representative examples from the range for *n*-values identified in Table 5. A similarity in the shape of CO_2 plume at the end of injection is observed for pairs of *n* that correspond to the same siliciclastic rock. Red ticks at the domains' horizontal boundaries in Fig. 5 illustrate plume edges at these boundaries for the defined *n*-value. The change in the shape of the CO_2 plume is attributed to the correlated structure of the rock matrix, which is described by the pore geometry parameter [*n*]. Smaller values for *n* increases the capillary resistance to buoyant migration of CO_2 plume, resulting in the preferentially lateral migration in the bottom of the modelled domain for lower *n*-values (Fig. 5). Through the same capillary resistance, the rate of snap-off of CO_2 ganglia at the trailing end of the plume, i.e. the residual trapping of CO_2, also increases, resulting in the lower degree of mobile gas saturation within the domain.

An assessment of the plume tip sensitivity was achieved through quantifying the total gas saturation at the end of CO_2 injection, for each *n*-value, in grid blocks at designated intervals on the bottom horizontal boundary (Table 6). The evaluation was implemented for only the bottom boundary due to larger variation in lateral plume migration at the base of the domain as observed in Fig. 5. To check the viability of *n*-values ranging from 1.01 to 1.09 in the description of hydraulic properties, a sensitivity study was conduction for this range using a constant $P_c - S_w$ relationship. Other reservoir parameters described in Section 4 remain applicable within varying $k_r - S_w$ relations based on the *n*-spectrum 1.01:0.01:1.10. Results show that CO_2 plume shapes correspond to $n = 1.11$ in Fig. 5, and the lateral migration of the plume goes beyond the radial distance of 500 m in the domain at the end of a 10-year CO_2 injection period (Fig. 6). It can be seen that data in Table 6 are similar to the range of *n*-values for different siliciclastic rocks presented in Fig. 4 and Table 5. This, in combination with Fig. 6, validates the representative *n*-values adopted for this study (see Table 3).

Radial distance along bottom boundary (m)	*Highest n-value showing CO_2 saturation*
50	3.00
75	2.33
100	1.98
150	1.67
200	1.53
250	1.43
300	1.35
350	1.28
400	1.22
450	1.16
500	1.12

Table 6: Correlation of CO_2 plume edge along the the base of the modelled domain for *n*-values

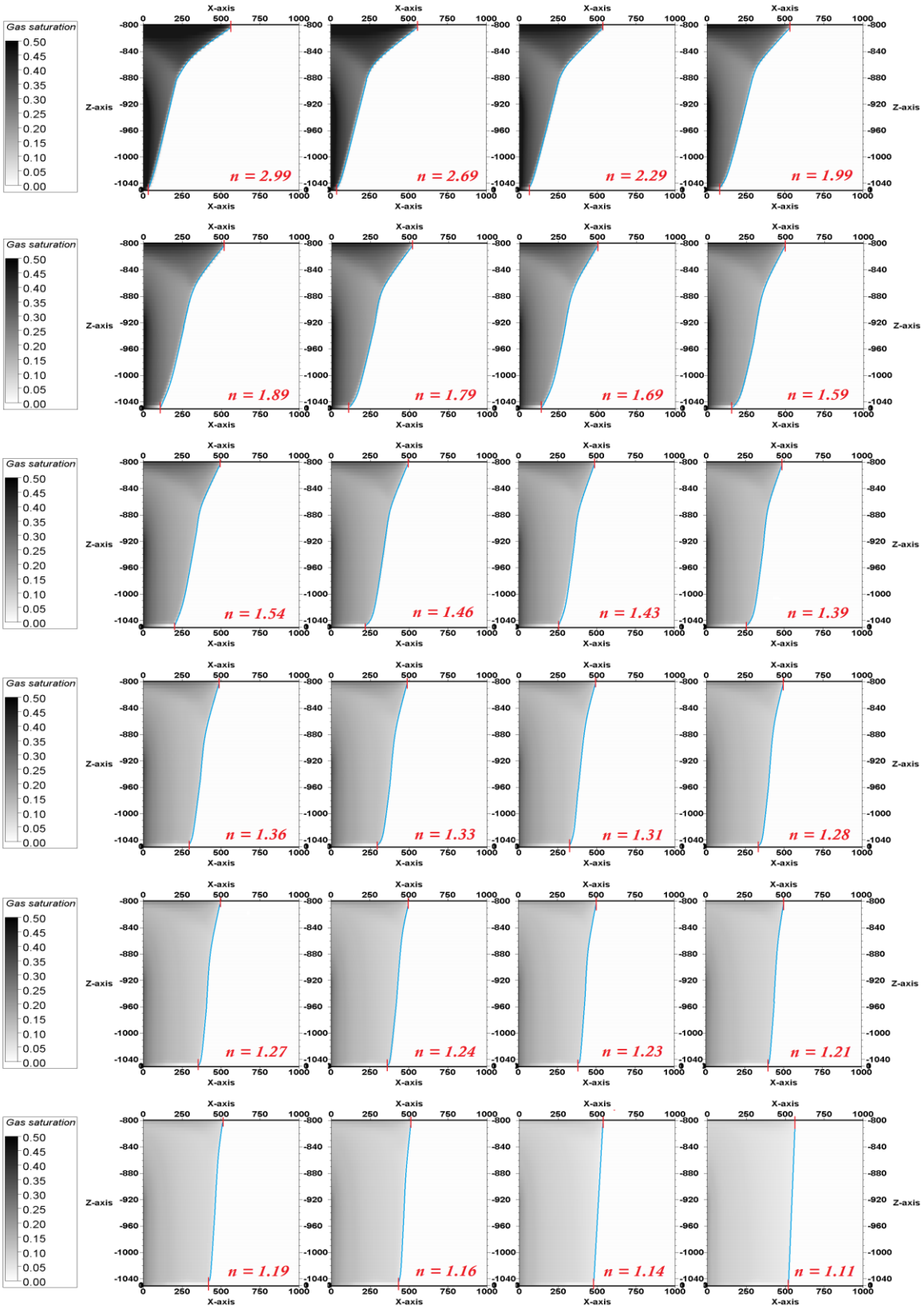

Fig. 5: The shape of CO_2 plume for representative examples of *n* at the end of simulation

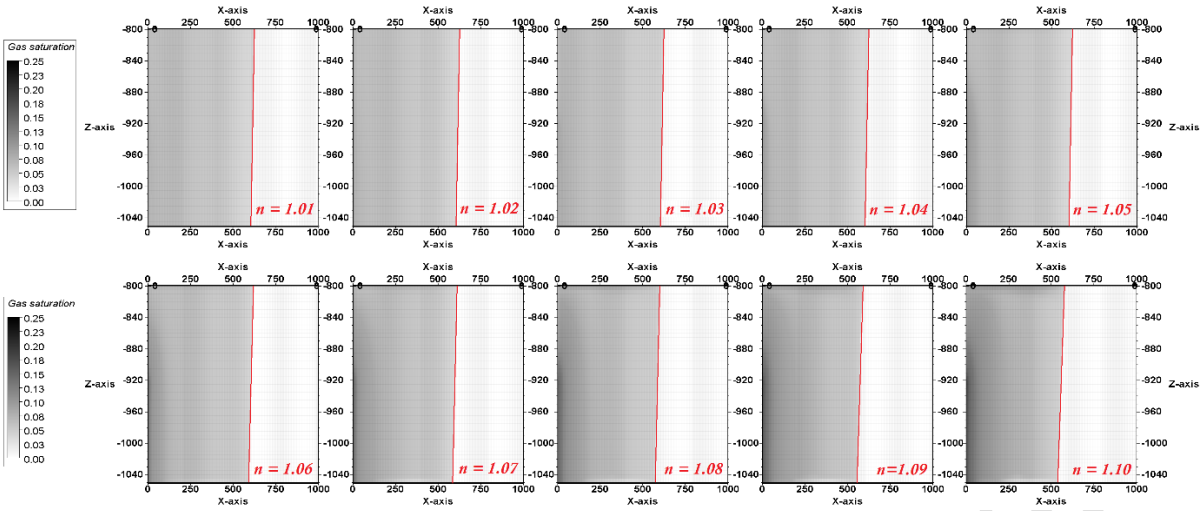

Fig. 6: CO_2 plume shape at the end of simulation for sensitivity study in the validity of *n*-values between 1.01 – 1.09 for describing hydraulic properties of siliciclastic rocks

5 Characterising empirical functions in vG-MC for CO_2 storage

The aquifer model used in this section is a three-dimensional (3D) isothermal and homogeneous domain (Fig. 7) discretised into 80 x 80 x 72 cells (460, 800 grid cells in total) and has dimensions of 2000 m x 2000 m x 220 m, which is comprised of a 10 m- and 210 m-thick caprock and reservoir formation, respectively. CO_2 injection was simulated using one vertical well centrally located in the model and perforated across layers 56 to 70 (approximately 60 m). The injector was set to operate at a target flow rate of 149,500 sm^3/day subject to a maximum bottom-hole pressure (BHP) of 23.62 MPa. This was specified to ensure that the hydrostatic pressure gradient in the model does not exceed the fracture pressure gradient, which was assumed to be 75% of the lithostatic pressure gradient. This and other petrophysical properties assumed for the flow simulation model are described in Table 7. Simulations were carried out using the compositional module of ECLIPSE (E300). In this section we address the relative impact of the pore geometry parameter [*n*], the residual wetting saturation [S_{wr}], the maximum non-wetting residual saturation [S_{nrmax}], and the description of P_c-curve on CO_2 storage in a homogeneous saline aquifer.

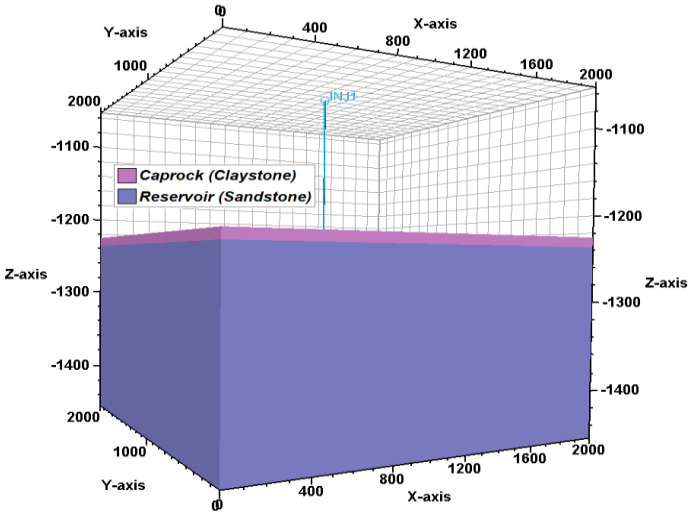

Fig. 7: Illustration of the 3D matrix aquifer model showing the caprock and reservoir formation.

Parameter	*Value in Caprock*	*Value in Reservoir*
Porosity	0.04	0.14
Permeability (mD)	6.30×10^{-3}	150
Capillary entry pressure (KPa)	172	1.622
Residual brine saturation	0.61	0.3
End-point relative permeability to CO_2	0.121	0.623
Maximum brine saturation	1.0	
End-point relative permeability to brine	1.0	
Temperature (°C)	33	
Brine salinity (ppm)	300,000	
Hydrostatic pressure gradient (KPa/m)	12.15	
Fracture pressure gradient (KPa/m)	16.97	

Table 7: Petrophysical properties used for the E300 simulations

5.1 Descriptions of P_c-curve: vG (for Pg ≠ Pe & Pg = Pe) vs BC

This section analyses the relative impact of the parametric description of capillary entry pressure in the vG model on flow simulation in a $scCO_2$/brine system. Here, Brooks-Corey description for capillary pressure is defined as the benchmark empirical model, idenitifed as *BC*, while two variations of vG's $P_c - S_w$ model are based on the following descriptions: i) the strength coefficient [P_g] is equivalent to the capillary entry pressure [P_e], where the model is identified as *vG (Pg = Pe)*, and ii) the strength coefficient is not equal to the capillary entry pressure but a derivative of the parameter equivalence between BC and vG shown in Eqn. 12, where the model is identified as *vG (Pg ≠ Pe)*. The value for capillary entry pressure [P_e] used for the reservoir is specified in Table 7 *i.e.* 1.62 KPa. Description of the relative permeability functions are based on the Mualem-Corey model (Eqn. 3 & 4) coupled to all three $P_c - S_w$ models identified herein. These capillary pressure curves are illustrated in Fig. 8.

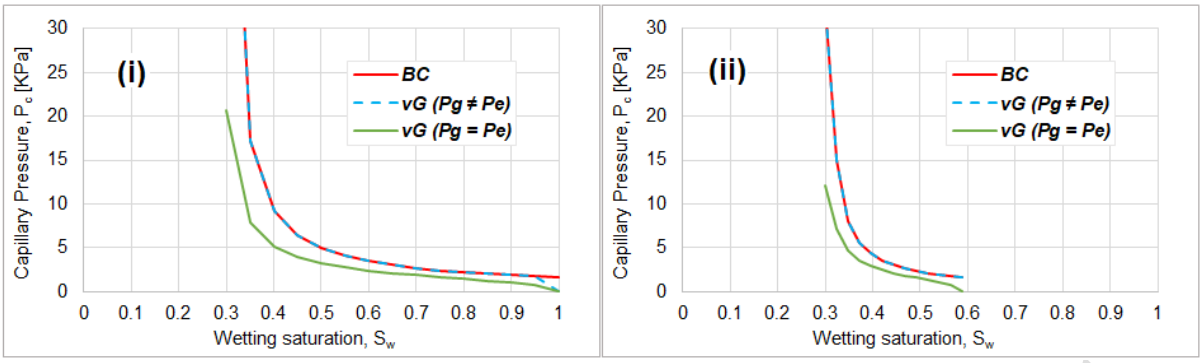

Fig. 8: Brooks-Corey (BC) and van Genuchten (vG) capillary pressure curves for (i) drainage and (ii) imbibition in the sandstone reservoir

During flow simulation, CO_2 injection rate is seen to be constant across all three cases until the seventh year of injection when it reaches the formation's limiting pressure and reduces drastically for each case. The reduction rate vary across the cases with *BC* showing the highest and *vG (Pg = Pe)* the lowest, thus influencing the cumulative CO_2 injected in each case (Fig. 9). The trend is attributed to the entry and exit point of the P_c drainage plot (Fig. 8i), where exit points for *BC* and *vG (Pg ≠ Pe)* are similar and greater than the exit point for *vG (Pg = Pe)*. This translates to higher resistance to drainage flow for the former over the latter. Hence the constrast in CO_2 injection rate post-decline between *BC* and *vG (Pg ≠ Pe)* can be ascribed to their varying entry points on the P_c-curve.

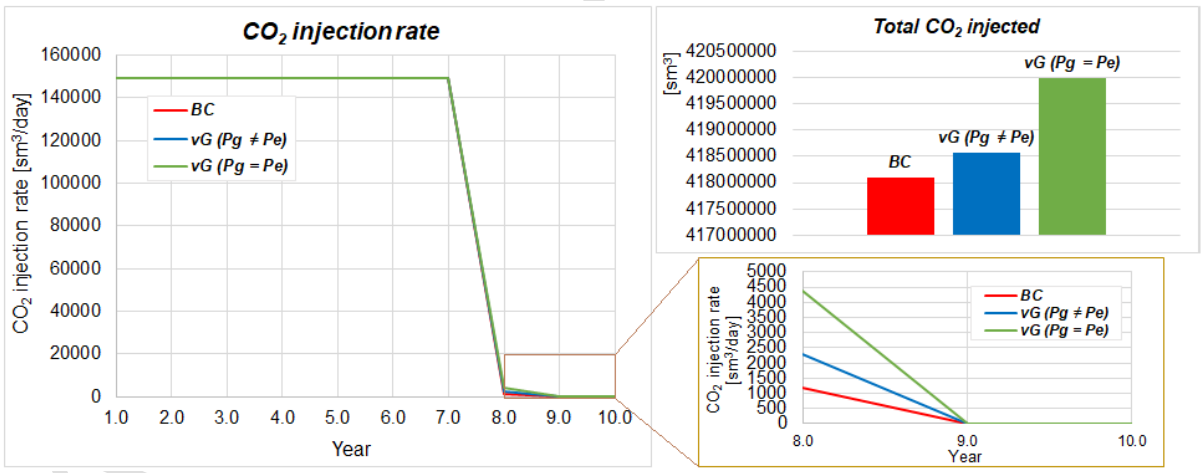

Fig. 9: Illustration of CO_2 injection rate and total CO_2 injection during flow simulation.

Although the *vG (Pg ≠ Pe)* and *BC* models are not entirely identical in terms of simulating the total CO_2 injected, the *vG (Pg ≠ Pe)* model exhibits a closer match to the *BC* model with an increase of 0.12% compared to 0.5% in the *vG (Pg = Pe)* model. In the seventh year of CO_2 injection where the cumulative gas injected is the same for all cases, the degree of primary trapping mechanisms also shows a close similarity between the *BC* and *vG (Pg ≠ Pe)* models (Fig. 10). The percentage of structurally trapped CO_2 (i.e. mobile CO_2) is slightly higher for the *BC* model than the *vG (Pg ≠ Pe)* model because of the entry point on the P_c-curve which is

higher for the former (Fig. 8i). This impedes the bouyant migration of CO_2 plume in the *BC* model more than in the *vG (Pg ≠ Pe)* model (Fig. 10b). However, for residual trapping trapping, the identical P_c imbibition curves for the *vG (Pg ≠ Pe)* and *BC* models corresponds to the equivalent percentage of residually trapped CO_2 in the seventh year of gas injection. The lower entry and exit points on the P_c imbibition curve for the *vG (Pg = Pe)* model results in additional capillary trapping of CO_2 (Fig. 10c) because more water readily imbibes into the pore matrix at lower capillary pressures. Fig. 10 indicates that the *BC* and *vG (Pg ≠ Pe)* models show an equal amount of residually trapped CO_2, which vary from the *vG (Pg = Pe)* model by approximately 2% of the total injected volume by the seventh year. This demonstrates a greater percentage error in CO_2 injection rate when the capillary entry pressure in vG is assumed to be the strength coefficient.

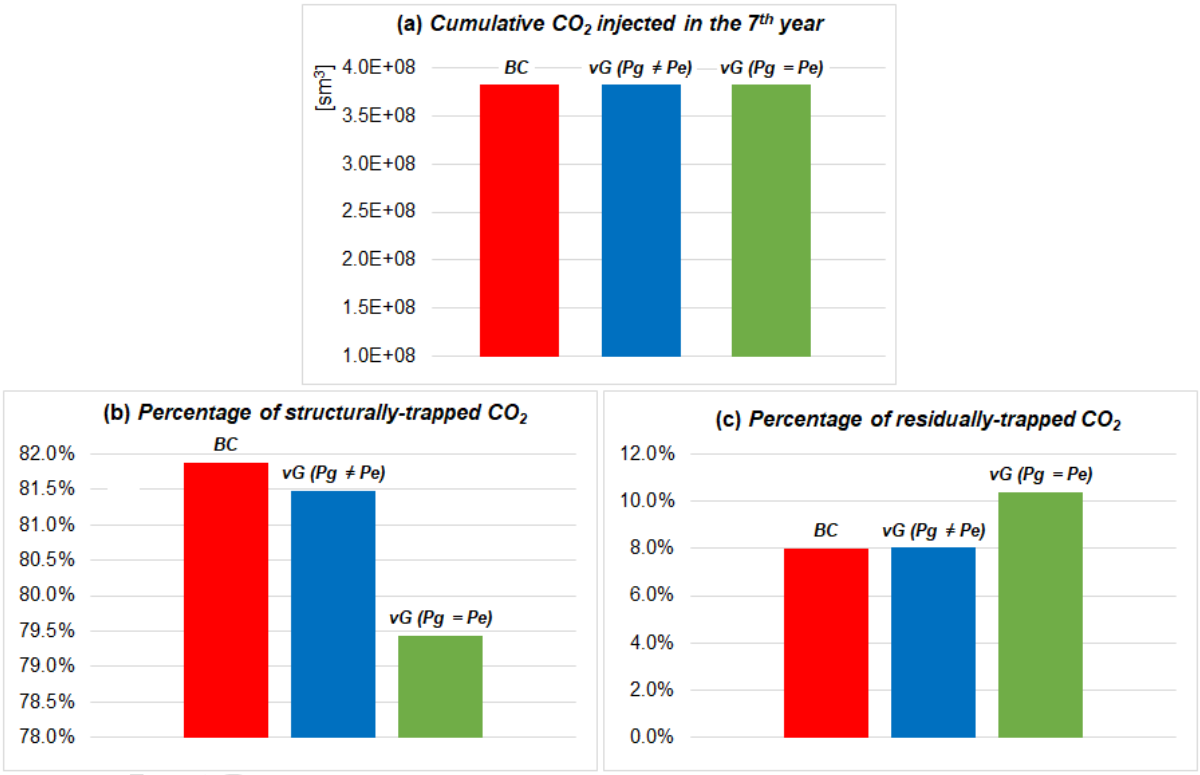

Fig. 10: Illustration of (a) the total volume of CO_2 sequestered in the 7th year of CO_2 injection by (b) structural, and (c) capillary trapping mechanisms.

5.2 CO_2 storage performance: *n* vs S_{wr} vs S_{nrmax}

This section highlights the relative importance of the pore geometry parameter, *n*, the residual wetting saturation [S_{wr}] and the maximum non-wetting residual saturation [S_{nrmax}] during the predictive analysis of CO_2 sequestration. The study is initialised with the vG-MC model where *vG ($P_g ≠ P_e$)* is identified as the base case, CASE 0. Different variations of relative permeability and capillary pressure based on assumed values for *n*, S_{wr}, and S_{nrmax} (as identified in Table

2) are computed using the vG-MC model and defined as CASE 1, 2, 3, X, Y & Z. In order to curb the mitigating effect of relative permeability on CO_2 injection, these k_r and P_c functions were imputed in the top-half of the reservoir formation, high above the well perforations, while the bottom-half of the reservoir had a constant k_r and P_c functions for all cases. Table 8 and Fig. 11 describe the design of the sensitivity study in this regard, where S_{wr} and S_{nrmax} values vary from 0.3 to 0.6, while n values vary from 1.56 to 2.67.

CASE ID (n-value)	***SUB-CASE*** *(Description)*		
CASE 0 (n=2.67)	**-** *(S_{wr} = 0.30; S_{nrmax} = 0.30)*		
CASE 1 (n=2.28)	***A*** *(P_c – S_w – k_r curves computed with representative n-value; S_{wr} = 0.30; S_{nrmax} = 0.30)*	***B*** *(k_r – S_w curve computed with representative n-value; P_c – S_w curve the same as BASE's; S_{wr} = 0.30; S_{nrmax} = 0.30)*	***C*** *(P_c – S_w curve computed with representative n-value; k_r – S_w curve the same as BASE's; S_{wr} = 0.30; S_{nrmax} = 0.30)*
CASE 2 (n=1.89)			
CASE 3 (n=1.56)			
CASE X (n=2.67; Vary S_{wr} & S_{nrmax})	***1*** *(S_{wr} = 0.35, S_{nrmax} = 0.35)*	***2*** *(S_{wr} = 0.40, S_{nrmax} = 0.40)*	***3*** *(S_{wr} = 0.45, S_{nrmax} = 0.45)*
CASE Y (n=2.67; Constant S_{wr})	***1*** *(S_{wr} = 0.30, S_{nrmax} = 0.40)*	***2*** *(S_{wr} = 0.30, S_{nrmax} = 0.50)*	***3*** *(S_{wr} = 0.30, S_{nrmax} = 0.60)*
CASE Z (n=2.67; Constant S_{nrmax})	***1*** *(S_{wr} = 0.40, S_{nrmax} = 0.30)*	***2*** *(S_{wr} = 0.50, S_{nrmax} = 0.30)*	***3*** *(S_{wr} = 0.60, S_{nrmax} = 0.30)*

Table 8: Sensitivity study design for addressing the relative impact of n, S_{wr}, and S_{nrmax} in CO_2 storage performance

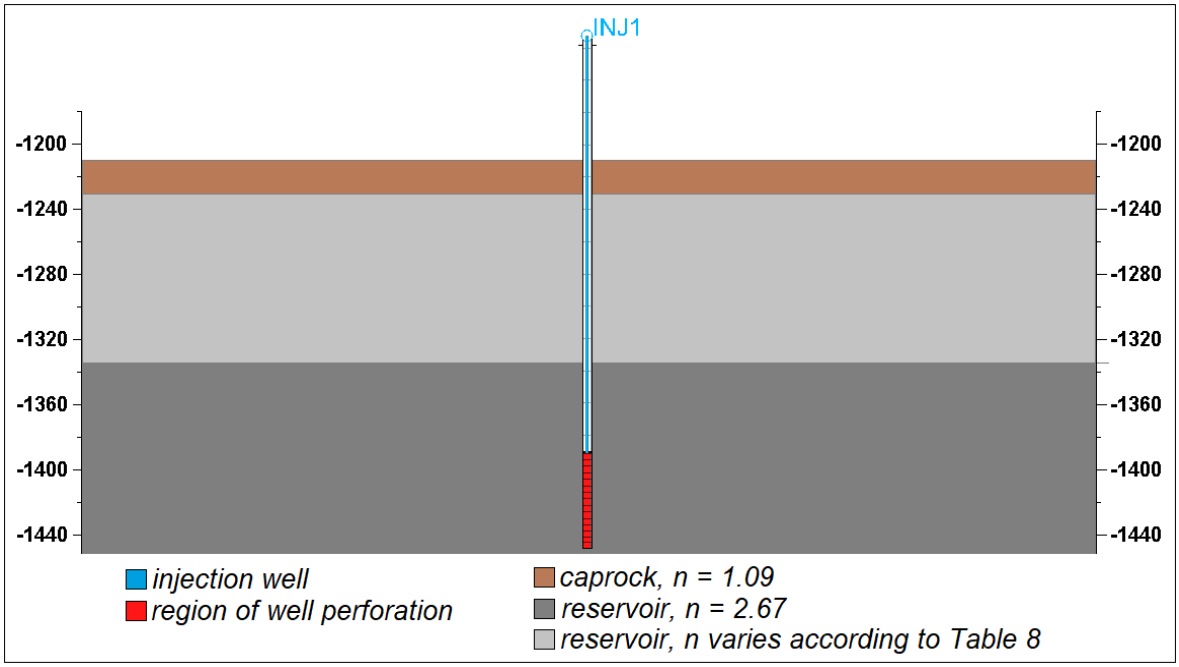

Fig. 11: Description of segments in the reservoir for variations according to Table 8.

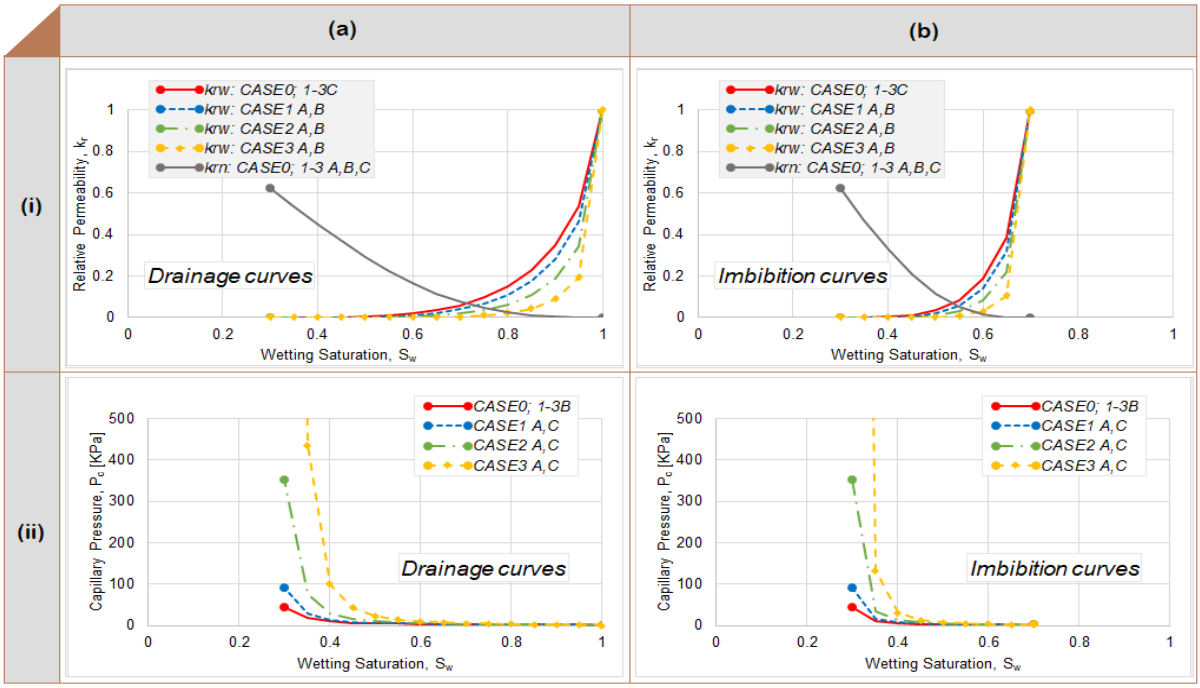

Fig. 12: P_c – S_w – k_r curves (a) drainage and (b) imbibition in all descriptions of CASEs 0, 1, 2 & 3

Fig. 12 shows the P_c – S_w – k_r relationship computed for CASE 0, 1, 2 & 3. From the vG-MC model (Eqns. 2 – 4) we know that pore geometry parameter has no effect on the relative permeability to the non-wetting phase, hence a single representative curve exists for all cases in Fig. 12. Nevertheless, n has a considerable effect on the relative permeability to the wetting phase and the capillary pressure. Conversely, S_{wr} and S_{nrmax} are seen to be significant in both functions of the relative permeability, i.e. k_{rw} and k_{rn}, where S_{wr} mainly influences the drainage curve and S_{nrmax} influences the imbibition curve (Fig. 13). Fig. 14 – 19 illustrate the degree of mobile and immobile CO_2 saturation at the end of a 10-year flow simulation, quantified as structurally trapped and residually trapped CO_2 respectively.

5.2.1 Analysis of S_{wr}

The impact of variation in values of the residual wetting saturation [S_{wr}] are described by CASE Z and illustrated in Fig. 14. Here the quantity of structurally trapped CO_2 at the end of simulation is highest in the base case (CASE 0) and progressively decreases in CASE Z from 1 to 3 (Fig. 14a). The reverse is the case for the residual trapping of the CO_2 plume in Fig. 14b, where the rate of CO_2 immobilisation in the rock matrix is seen to be directly proportional to S_{wr}. The higher the S_{wr}, the lower the measure of continuously mobile saturation of CO_2 that is available to be structurally trapped by flow barriers in the reservoir model. This is because increasing the S_{wr} increases the wettability of the rock matrix, i.e. its affinity to the wetting fluid. This feature is portrayed in the k_r – S_w drainage curves where the intercept of both functions shift to the higher end of the wetting saturation as S_{wr} increases (Fig. 13a-iii). Consequently, the displacement efficiency of the wetting phase by the invading CO_2 diminishes.

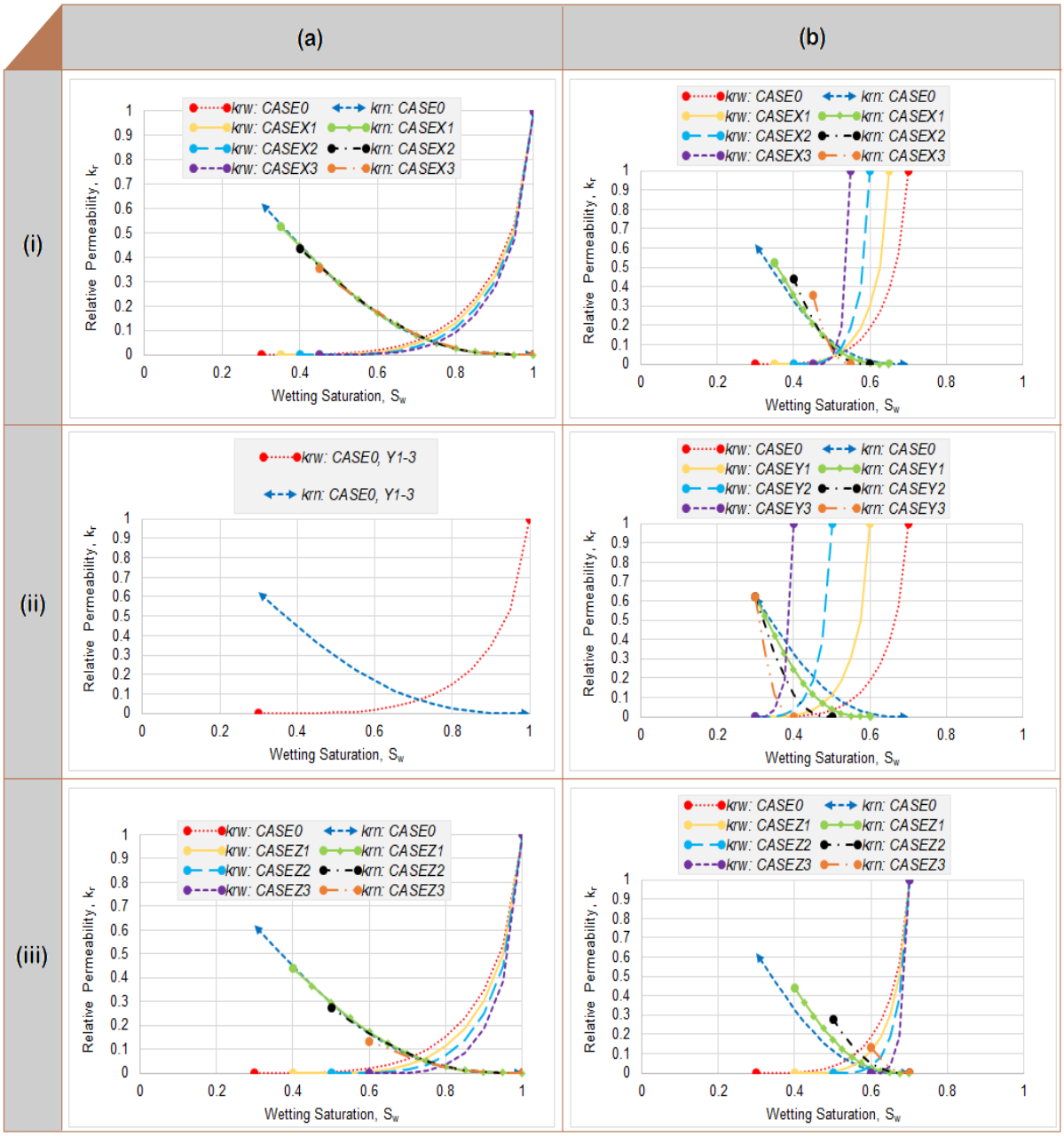

Fig. 13: k_r – S_w curves for (a) drainage and (b) imbibition in all descriptions of CASE 0 vs i) CASE X, ii) CASE Y, and iii) CASE Z.

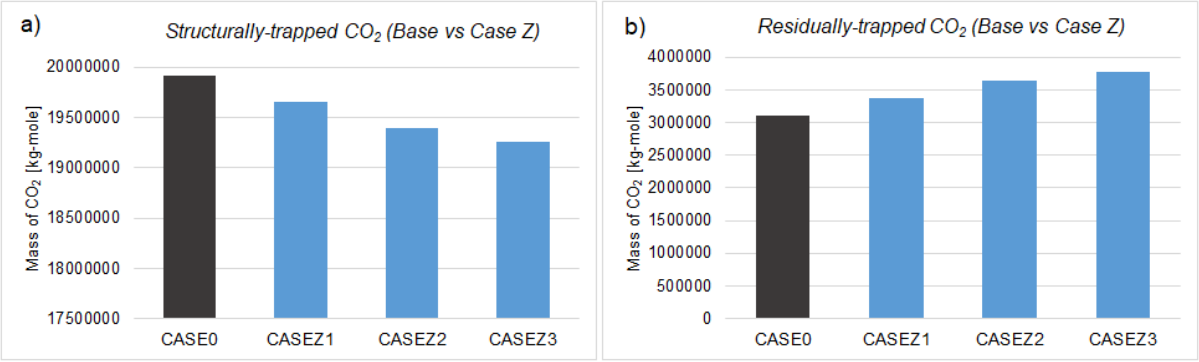

Fig. 14: Quantity of CO_2 sequestered by (a) structural, and (b) residual trapping mechanisms at the end of gas injection for the base case and all descriptions of CASE Z.

5.2.2 Analysis of S_{nrmax}

The impact of variation in values of the maximum residual non-wetting saturation [S_{nrmax}] are described by CASE Y and illustrated in Fig. 15. Here the quantity of structurally trapped CO_2 decreases as the value of S_{nrmax} increases. This is mainly attributed to the capillary trapping efficiency, defined by the imbibition curves in Fig. 13b-ii, which increases with increasing S_{nrmax} thereby inducing the immobilisation of more CO_2 particles. This invariably results in the higher quantity of mobile CO_2 for the smallest value of S_{nrmax}, i.e. CASE 0 (Fig. 15a), irrespective of the single k_r – S_w drainage curve defined for CASE 0, Y1, Y2 & Y3 (Fig. 13a-ii).

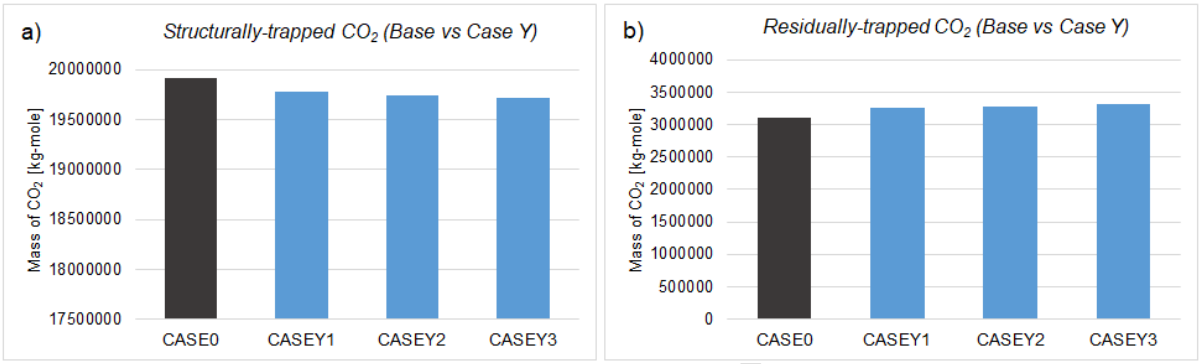

Fig. 15: Quantity of CO_2 sequestered by (a) structural, and (b) residual trapping mechanisms at the end of gas injection for the base case and all descriptions of CASE Y.

When both values of S_{wr} and S_{nrmax} are increased simultaneously, as portrayed by CASE X in Table 8, the progressive decrease in the quantity of CO_2 structural trapped (see Fig. 16a) is accredited to the increasing S_{wr}, while the increase in the residual trapping of CO_2 (see Fig. 16b) is mainly a function of the increasing S_{nrmax}.

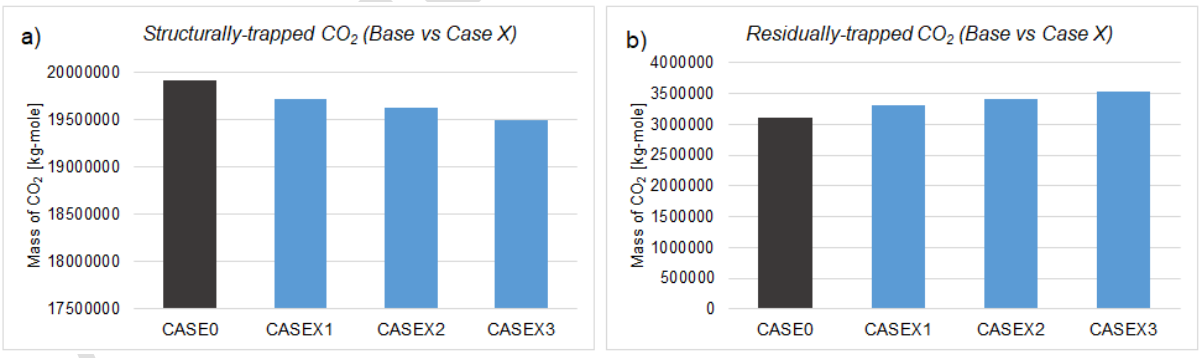

Fig. 16: Quantity of CO_2 sequestered by (a) structural, and (b) residual trapping mechanisms at the end of gas injection for the base case and all descriptions of CASE X

The S_{wr} can be said to work in tandem with the S_{nrmax}. Fig. 17 elaborates on this using a comparison of the mass of mobile CO_2 saturation quantified at the end of simulation for the base case and representative cases for X, Y, & Z that aids the comparability, namely: CASE X2, Y1 & Z1. Using the base case, CASE 0, as a reference point in Fig. 17, the disparity in the mass of structurally trapped CO_2 at the end of simulation is highest in CASE X2 due to the

simultaneous changes in S_{wr} and S_{nrmax}. Additionally, S_{wr} is seen to have a higher impact on the structural trapping of CO_2 than S_{nrmax} through a higher percentage change between CASE 0 and CASE Z1 than between CASE 0 and CASE Y1.

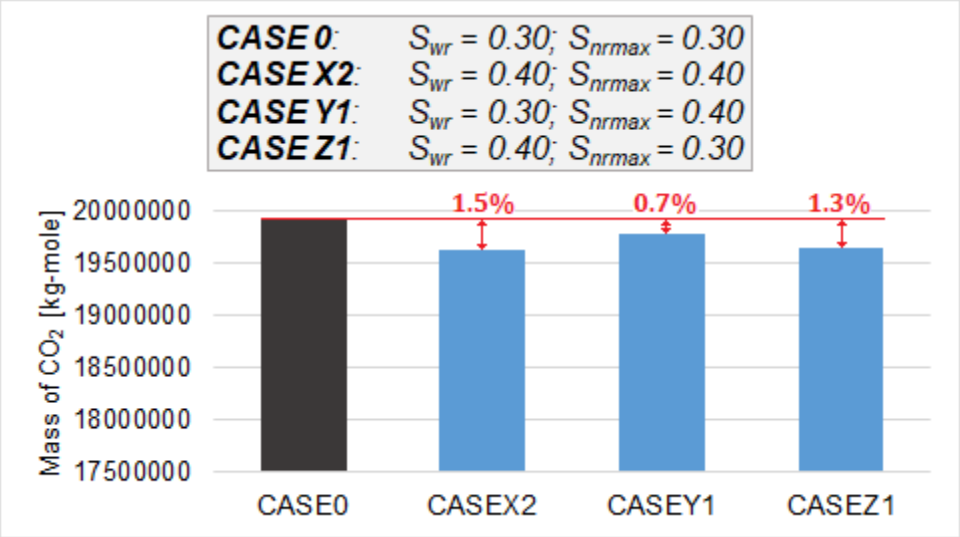

Fig. 17: Quantity of CO_2 in mobile gas phase at the end of gas injection for CASE 0, CASE X2, CASE Y1 and CASE Z1. NB: Using the base case as a reference point, the values highlighted in red show the percentage change in mass of structurally trapped CO_2 at the end of a 10-year CO_2 injection period.

5.2.3 Analysis of n

All descriptions of CASE 1, 2, & 3 describe the impact of variation in values for the pore geometry index [*n*]. In the sub-categories: A, B, & C, the variance in *n* was defined by the $P_c - S_w - k_r$, $k_r - S_w$, *and* $P_c - S_w$ curves, respectively. This means that for cases defined by A, the variability in *n*-values was incorporated into the $k_r - S_w$, *and* $P_c - S_w$ curves. Cases defined by B had variance in *n*-values only incorporated into the $k_r - S_w$ curves, while the difference in *n*-values was only incorporated into the $P_c - S_w$ curves of cases defined by C. Consequently, cases B were modelled with the same $P_c - S_w$ curve of the base case, which has the highest value for *n*, while C cases were modelled with the same $k_r - S_w$ curves as the base case. Otherwise both the magnitude of capillary pressure and wetting saturation at the intercept of the $k_r - S_w$ curves are lowest in the base case, CASE 0, and increases progressively from CASE 1 to CASE 3 (Fig. 12). This change in the shape of the relative permeability and capillary pressure curve, as a function of *n*, is attributed to the description of *n*-values in the van Genuchten model for clastic rocks, where higher values denote coarser-grained clasts (see Table 3). Thus coarser-grained clastic rocks, in comparison to their finer-grained counterparts, will possess a lower force of resistance to the buoyant migration of CO_2 plume and a higher relative permeability to the invading non-wetting gas. Likewise, the finer-grained clastic rocks, in comparison to their coarser-grained counterparts, will increase the capillary trapping efficiency of the rock matrix while also reducing the relative permeability to the CO_2 plume.

This explains why the mass of structurally trapped CO_2 decreases and the residual trapping efficiency increases with decreasing *n*, as illustrated in Fig. 18.

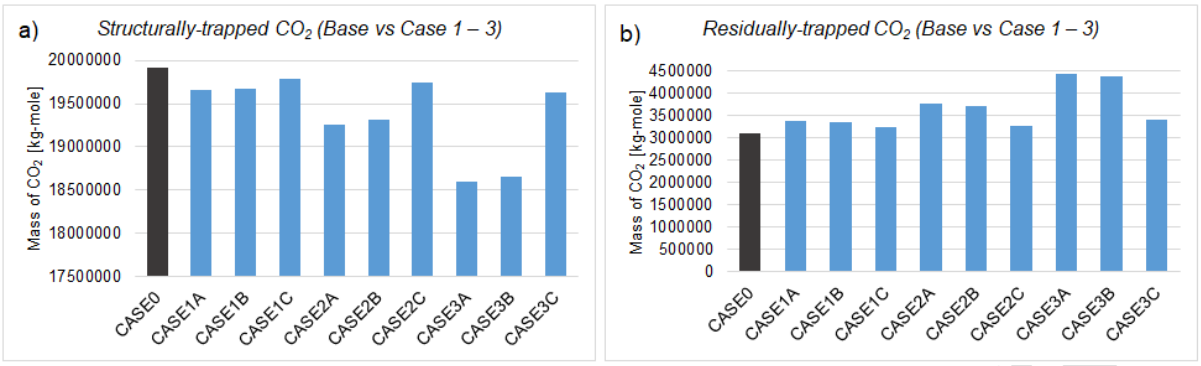

Fig. 18: Quantity of CO_2 sequestered by (a) structural, and (b) residual trapping mechanisms at the end of gas injection for all descriptions of CASE 0, 1, 2, & 3.

The sub-categories of CASE 1, 2 & 3, i.e. A, B & C, also show variation in the degree of mobile and immobile CO_2 at the end of simulation. The mass of structural trapped CO_2 is greatest in sub-categorised cases of C and smallest in A. For C-cases, the relative permeability functions lead to a higher rate of CO_2 mobility, which creates a preferential flow pathway that evades the fine-grained sedimentation within the rock fabric. These fine-grained sediments serve as possible snap-off regions in the porous media. In B-cases the transport properties of *in-situ* fluids imitate movement through the fine-grained sediments even though the resistant force to plume migration, i.e. capillary pressure functions, is lower here than in C. Hence, the slower moving CO_2 plume results in a lesser amount of structurally trapped CO_2 due to a higher degree of residual trapping within regions of finer-grained sedimentation. The mobility of CO_2 is lowest in A-cases because the flow transport properties and resistant force imitate percolation through fine-grained sedimentation. The higher resistant force acting on slower moving CO_2 plume results in a greater resident time of the non-wetting fluid in the constricted rock matrix. This increases the rate of CO_2 ganglia that is isolated from the migrating plume, thus making residual trapping highest for sub-categorised cases of A.

5.2.4 The relative impact of n, S_{wr} and S_{nrmax} on the CO_2 storage performance

Quantifying the degree of structural trapping at the end of the flow simulation show that a variance in the pore geometry parameter [*n*] has a higher impact on CO_2 storage performance than a variance in the residual wetting saturation [S_{wr}] and the maximum residual non-wetting saturation [S_{nrmax}]. This is illustrated in Fig. 19 where the bars indicating the amount of mobile CO_2 for cases with different *n* show greater variance from the base case than those for cases with different S_{wr} and S_{nrmax}. This is because the pore geometry of the rock essentially dictates the degree of residual wetting saturation and the maximum residual non-wetting saturation that could exist within its porous fabric. This accentuates the importance of the pore geometry parameter in subsurface flow simulation and the relevance of the concept of assigning different

values of n to different sedimentary rocks. To verify this assertion, Section 5.3 considers the influence of n in an aquitard on flow performance during CO_2 sequestration.

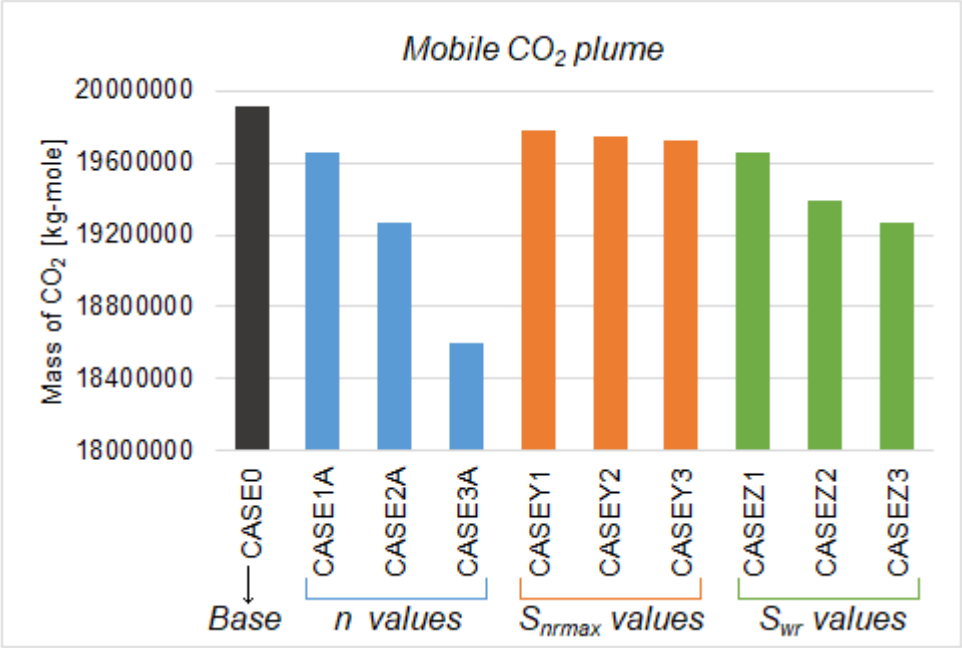

Fig. 19: Computing the impact of n, S_{wr} and S_{nrmax} on the mass of mobile CO_2 in gas phase at the end of a 10-year CO_2 injection period

5.3 Effect of *n* description in shale aquitard

Here we consider the same injection scheme for two variations of the base case. The first, CASE 0, as defined in the previous section and the second CASE V, which varies from CASE 0 through the description of the $P_c - S_w - k_r$ relationship in the caprock, where n = 1.56. The CO_2 injection rate and all other petrophysical parameters shown in Table 7 remain the same. Flow simulation is initialised for ten years of gas injection and an additional 40 years post gas injection. Fig. 20 depicts the quantity of CO_2 in the caprock at the end of the simulation, where the cumulative gas injection is equivalent for both cases. Results show a larger quantity of CO_2 in the caprock for CASE V, which indicates a higher relative permeability to the non-wetting CO_2 in CASE V in comparison to CASE 0. This is evident in the pressurisation of the caprock as illustrated in Fig. 21 where pressure magnitude around the injection well is greater for CASE V and transmits to the top of the caprock in the said case unlike CASE 0. Hence, for multiphase flow modelling in CO_2/brine/rock systems the pore geometry parameter [n] can influence the degree of trapping mechanisms and the pore pressure profile in the aquifer and the aquitard. This augments the importance of the parametric description of pore geometry index in CO_2/brine flow simulation that use empirical correlations such as the Brooks-Corey or the van Genuchten model to compute the $P_c - k_r - S_w$ relationships.

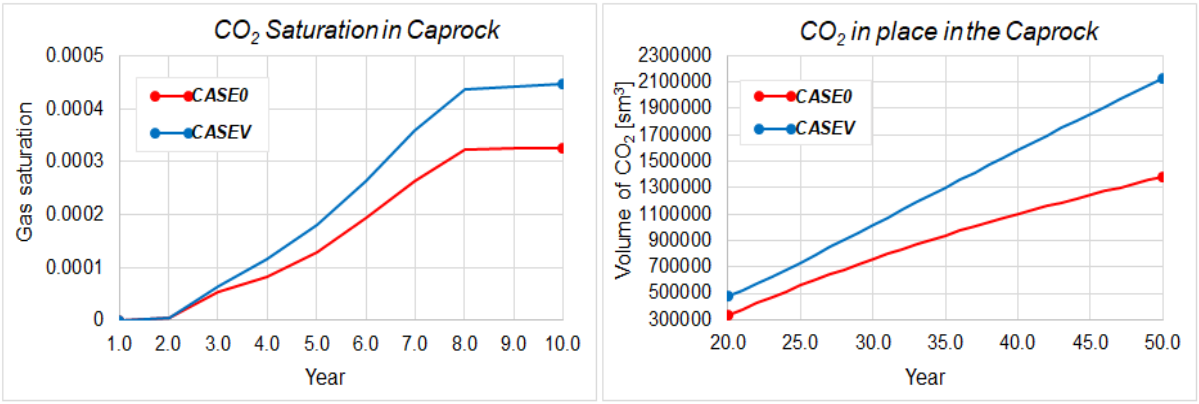

Fig. 20: Quantity of CO_2 in caprock at the end of a 10-year flow simulation

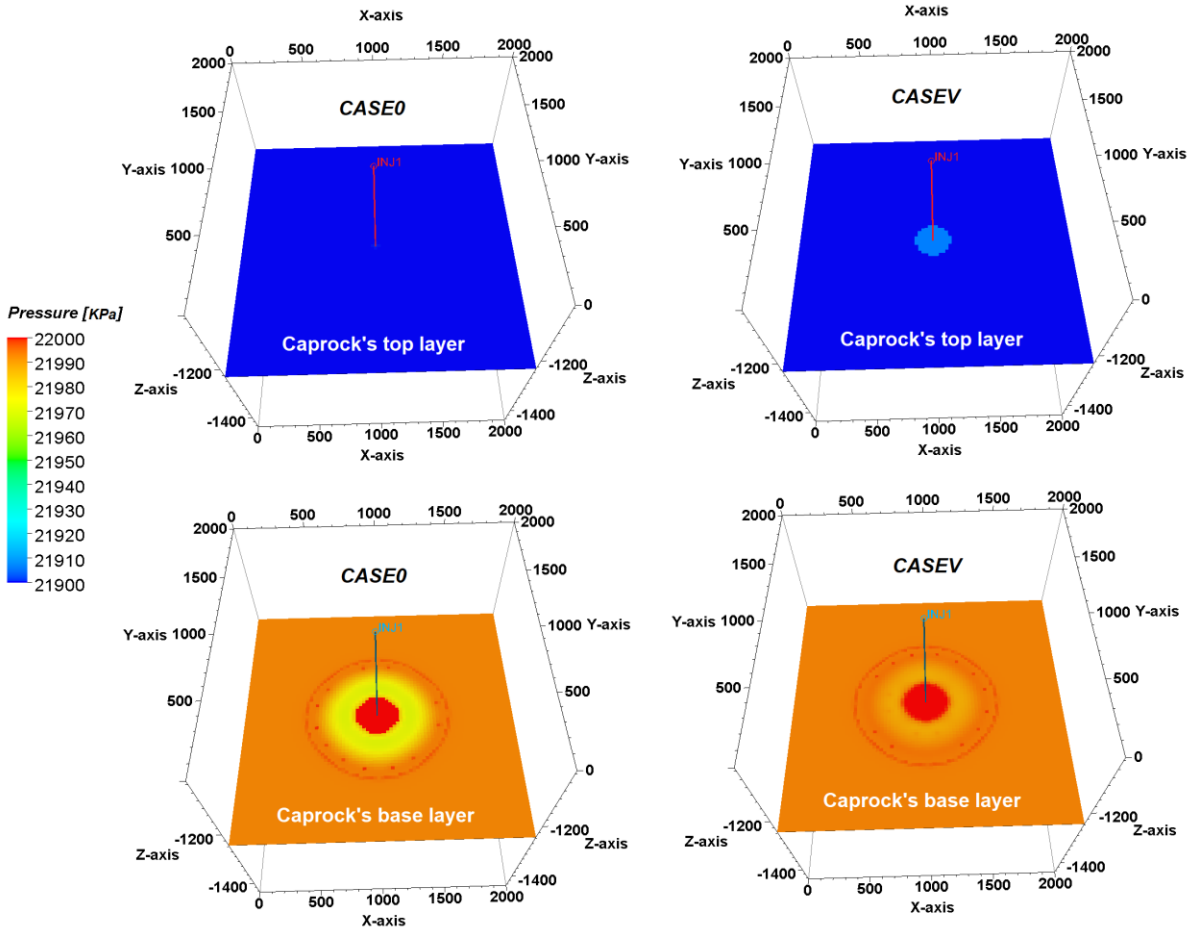

Fig. 21: Comparison of caprock pressurisation in CASE 0 and CASE V

6 Concluding remarks

In reservoir simulation studies, geologial heterogeneities are usually described by variations in permeability and porosity distribution, while variability in relative permeability [k_r] and capillary pressure [P_c] functions are easily overlooked e.g. Ambrose et al. (2008), Doughty and Preuss (2004). However, the choices of k_r and P_c functions are very important in experimental and numerical observations of CO_2 injection in a porous media with sedimentary

heterogeneities (Gershenzon et al., 2016; Sakaki et al., 2013). Due to the lack of experimental data for these functions, mainly because they are highly site specific and experimental validation is time consuming, emprical models such as Brooks-Corey (BC) and van Genuchten (vG) that describe k_r and P_c as a function of the wetting saturation [S_w] are used in the dynamic flow modelling of CO_2 geo-sequestration. For P_c – S_w curves, the BC model accounts for a non-zero capillary entry pressure while the vG model connects the entry slope of the curve to a capillary pressure of zero and fails to account for the entry capillary pressure. Capillary entry pressure is governed by the rock's wettability, the largest pore throat radius of the rock matrix, and the interfacial tension acting between the *in-situ* fluids and rock surface, making it an essential parameter in the derivation of P_c – S_w curves. In this paper, the relationship adopted for the equivalence of P_c – S_w curves in both models is described. The study is then extended to define the pore geometry parameter [*n*] in the vG model for different siliciclastic rocks. A quantitative methodology is presented to compare the contribution of 200 *n*-values, ranging from 1.01 to 3.00 with an increment of 0.01, on the uncertainty of CO_2 plume evolution in a homogeneous saline aquifer. The methodology accounts for both the degree of uncertainty in each value and the application of a representative parametric value for a range of *n*. Four ranking criteria were outlined when comparing parameter roles in the uncertainty of CO_2 plume evolution at the end of a 10-year scCO_2 injection period:

i. The shape of CO_2 plume.
ii. Plume edge at the bottom of the modelled domain.
iii. Fraction of mobile CO_2 saturation.
iv. Percentage volume of residual CO_2.

According to all four criteria, the pore geometry index clearly influences the uncertainty in the migration and trapping behaviour of the CO_2 plume. Results show that the parameterisation scheme for *n*-values described by Carsel and Parrish (1988) in soil physics can be applicable in rock physics. Furthermore, the primary parameters of the van Genutchen model, i.e the pore gemetry index [*n*], the residual wetting saturation [S_{wr}] and the maximum residual non-wetting saturation [S_{nrmax}], are individually characterised to identify their relative impact on predictive analyis of CO_2 storage. Low values in *n*, S_{wr} and S_{nrmax} lead to increased gas migration while high values lead to increased immobilisation of the CO_2 plume. Among the three parameters within the parameter range investigated in this work, *n* is identified as the most significant element in the simulation and analysis of CO_2/brine flow in subsurface storage media, hence the significance of assigning defined values of *n* to different sedimentary rocks. This is because the pore geometry index dictates the degree of S_{wr} and S_{nrmax} that can exist in the a rock's matrix. In realistic geological settings, the highly compacted pore geometry of finer-grained rocks will, most likely, restrict fluid perolation and increase in-situ fluid retention to a higher degree than the less compacted pore geometry of coarser-grained rocks.

Using the same n value when computing the $P_c - k_r - S_w$ relationship for siliciclastic rocks that make up the storage formation, such as sandstones, and those that make up the sealing formation, such as mudstones, can curb the accuracy in the forward modelling of CO_2 storage performance. In the absence of site-specific data on capillary pressure, relative permeability and pore geometry distribution, the study proposes a parameterisation scheme for the pore geometry index that can serve as a tool for modelling hydraulic heterogeneities in clastic formations. For the sake of a comprehensive demonstration, this methodology has been applied to flow simulation through stratigraphic heterogeneities such as graded bedding in the reservoir (Onoja and Shariatipour, 2018) and transitional lithologies in the seal (Onoja et al., 2019). The authors observed that the exclusion of relative permeability and capillary heterogeneities in the dynamic modelling of CO_2 sequestration can underestimate the storage performance of the reservoir and the seal. This methodology can be adapted for history-matching CO_2 distribution in large scale storage projects, such as the Sleipner gas project in Norway which injects CO_2 into the Utsira Sand Formation with interbedded mudstones (Arts et al., 2004). Using the theoretical approach of this parameterisation scheme to describe the k_r and P_c functions for the varying clastic units in this formation could improve the understanding of plume migration pattern in Sleipner's Benchmark Model (Singh et al., 2010). Addtionally, petrographic data obtained from the lithological information from boreholes that are used to develop the structural and lithological model for pilot CO_2 storage demonstration projects can also be used to describe the P_c and k_r functions using this parameterisation scheme.

Acknowledgements

This paper is based upon work supported by Coventry University's Fluid and Complex Systems Research Centre. We appreciate the constructive input of Dr. Philip Costen, and thank Schlumberger for the use of ECLIPSE and Petrel Software.

Appendix A.

```
i=1;
SOF2d =zeros(15,2,200);
SGFNd =zeros(15,3,200);
SOF2i =zeros(13,2,200);
SGFNi =zeros(13,3,200);
for n=1.01:0.01:3;

%DRAINAGE
 jd=1;

 for sw=0.3:0.05:1;
 m=1-1/n;
 lan=m/(1-m)*(1-0.5^(1/m));
 sew=(sw-0.3)/(1-0.3);
 pc(jd)=0.01622/sew^(1/lan);
 krw(jd)=sew^0.5*(1-(1-sew^(1/m))^m)^2;
 krg(jd)=0.623*(1-sew)^2*(1-sew^2);
 sw(jd)=sw;

 SOF2d (jd,1,i)=sw(jd);
 SOF2d (jd,2,i)=krw(jd);
 SGFNd (16-jd,1,i)=1-sw(jd);
 SGFNd (16-jd,2,i)=krg(jd);
 SGFNd (16-jd,3,i)=pc(jd);

 jd=jd+1;

end

%IMBIBITION
 ji=1;

 for sw=0.3:0.024:0.588;
 m=1-1/n;
 lan=m/(1-m)*(1-0.5^(1/m));
 sew=(sw-0.3)/(0.588-0.3);
 pc(ji)=0.01622/sew^(1/lan);
 krw(ji)=sew^0.5*(1-(1-sew^(1/m))^m)^2;
 krg(ji)=0.623*(1-sew)^2*(1-sew^2);
 sw(ji)=sw;

 SOF2i (ji,1,i)=sw(ji);
 SOF2i (ji,2,i)=krw(ji);
 SGFNi (14-ji,1,i)=1-sw(ji);
 SGFNi (14-ji,2,i)=krg(ji);
 SGFNi (14-ji,3,i)=pc(ji);

 ji=ji+1;

end
```

```
%% …CONTINUATION
%% print_file
cd file_location;
fid=fopen('kr.inc','w');

fprintf(fid,'SGFN \n');

SGFNd_T=transpose(SGFNd(:,:,i));
fprintf(fid,'%f %f %f\r\n',SGFNd_T);
fprintf(fid,'\n/');
fprintf(fid,'\n');

SGFNi_T=transpose(SGFNi(:,:,i));
fprintf(fid,'%f %f %f\r\n',SGFNi_T);
fprintf(fid,'\n/');
fprintf(fid,'\n');
fprintf(fid,'SOF2 \n');

SOFTd_T=transpose(SOF2d(:,:,i));
fprintf(fid,'%f %f\r\n',SOFTd_T);
fprintf(fid,'\n/');
fprintf(fid,'\n');
SOFTi_T=transpose(SOF2i(:,:,i));
fprintf(fid,'%f %f\r\n',SOFTi_T);
fprintf(fid,'\n/');
fclose(fid);

%% RUN
nn=num2str(n);
foldername=['n_' nn '.data'];
mkdir(foldername)
copyfile('BASE.data',foldername)
copyfile('MULTPV.inc',foldername)
copyfile('PROPS_FLUID.INC',foldername)
copyfile('summary.inc',foldername)
copyfile('TRANX.inc',foldername)
copyfile('TRANZ.inc',foldername)
copyfile('kr.inc',foldername)
copyfile('$eclipse.bat',foldername)
cd(['./' foldername])
movefile('BASE.data',foldername)
input_file=foldername;
[~, fName, ext] =
fileparts(input_file);
aaa=['$eclipse.bat ' fName];
system(aaa);

i=i+1;

end
```

Algorithm A1: MATLAB-code used to compute P_c – k_r – S_w data and initialise reservoir simulation in E100

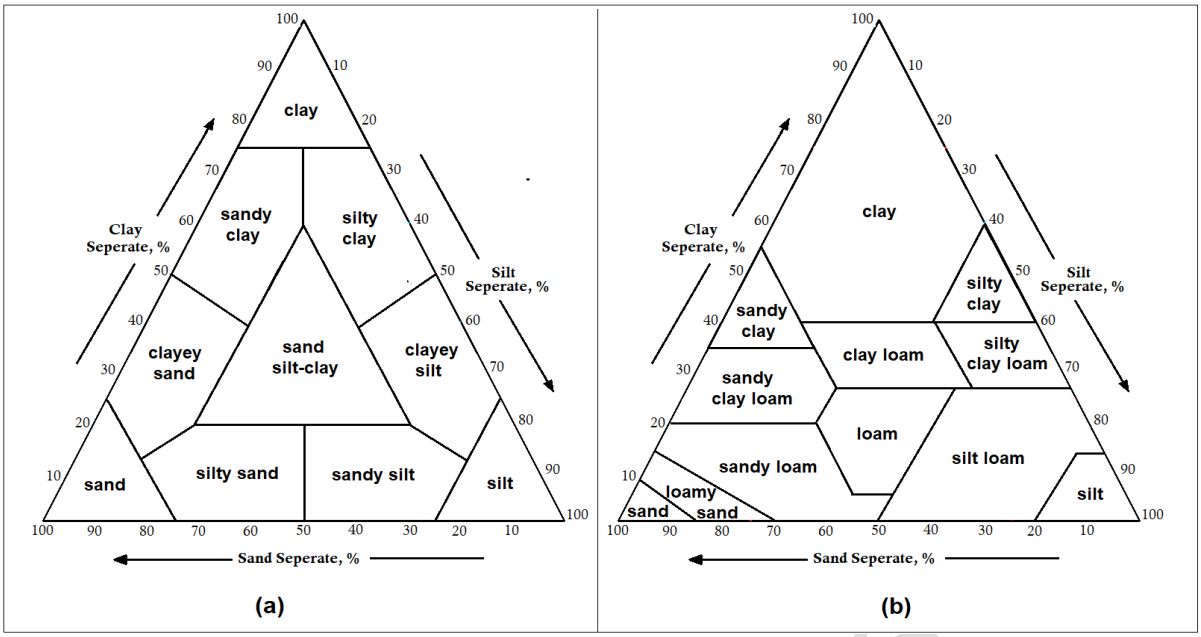

Fig. A1: Ternary diagram of (a) the recommended conceptual scheme for the nomenclature of mixed clastic sediments, and (b) USDA's soil textural classification.

References

Ambrose, W.A., Lakshminarasimhan, S., Holtz, M.H., Núñez-López, V., Hovorka, S.D., Duncan, I., 2008. Geologic factors controlling CO2 storage capacity and permanence: case studies based on experience with heterogeneity in oil and gas reservoirs applied to CO2 storage. Environ Geol 54, 1619–1633. https://doi.org/10.1007/s00254-007-0940-2

Aplin, A.C., Fleet, A.J., Macquaker, J.H.S., 1999. Muds and mudstones: physical and fluid-flow properties, Geological Society special publication. Geological Society; USA distributor, AAPG Bookstore, London; Tulsa, OK.

Arts, R., Eiken, O., Chadwick, A., Zweigel, P., van der Meer, L., Zinszner, B., 2004. Monitoring of CO2 injected at Sleipner using time-lapse seismic data. Energy 29, 1383–1392. https://doi.org/10.1016/J.ENERGY.2004.03.072

Bachu, S., 2013. Drainage and Imbibition CO2/Brine Relative Permeability Curves at in Situ Conditions for Sandstone Formations in Western Canada. Energy Procedia 37, 4428–4436. https://doi.org/10.1016/J.EGYPRO.2013.07.001

Birkholzer, J.T., Oldenburg, C.M., Zhou, Q., 2015. CO2 migration and pressure evolution in deep saline aquifers. Int J Greenh Gas Control 40, 203–220. https://doi.org/http://dx.doi.org/10.1016/j.ijggc.2015.03.022

Birkholzer, J.T., Zhou, Q., Tsang, C.-F., 2009. Large-scale impact of CO2 storage in deep saline aquifers: A sensitivity study on pressure response in stratified systems. Int J Greenh Gas Control 3, 181–194. https://doi.org/10.1016/J.IJGGC.2008.08.002

Boggs, S., 2009. Petrology of sedimentary rocks, 2nd ed. Cambridge University Press, Cambridge.

630 Brooks, R.H., Corey, A.T., 1964. Hydraulic properties of porous media. Hydrol Pap.

631 BSI, 1990. British Standard Methods of Test for Soils for Civil Engineering Purposes. BS
632 1377: Part 1-9. British Standards Institution.

633 Carsel, R.F., Parrish, R.S., 1988. Developing joint probability distributions of soil water
634 retention characteristics. Water Resour Res 24, 755–769.
635 https://doi.org/10.1029/WR024i005p00755

636 Dewhurst, D.N., Aplin, A.C., Sarda, J.-P., Yang, Y., 1998. Compaction-driven evolution of
637 porosity and permeability in natural mudstones: An experimental study. J Geophys Res
638 Solid Earth 103, 651–661. https://doi.org/10.1029/97JB02540

639 Doughty, C., 2010. Investigation of CO2 Plume Behavior for a Large-Scale Pilot Test of
640 Geologic Carbon Storage in a Saline Formation. Transp Porous Media 82, 49–76.
641 https://doi.org/10.1007/s11242-009-9396-z

642 Doughty, C., Freifeld, B.M., Trautz, R.C., 2008. Site characterization for CO2 geologic
643 storage and vice versa: the Frio brine pilot, Texas, USA as a case study. Environ Geol
644 54, 1635–1656. https://doi.org/10.1007/s00254-007-0942-0

645 Doughty, C., Pruess, K., 2004. Modeling supercritical carbon dioxide injection in
646 heterogeneous porous media. Vadose Zo J 3, 837–847.

647 Dullien, F.A.L., 1991. Porous Media: Fluid Transport and Pore Structure., 2nd ed. Academic
648 Press.

649 Espinet, A., Shoemaker, C., Doughty, C., 2013. Estimation of plume distribution for carbon
650 sequestration using parameter estimation with limited monitoring data. Water Resour
651 Res 49, 4442–4464. https://doi.org/10.1002/wrcr.20326

652 Flemming, B.W., 2000. A revised textural classification of gravel-free muddy sediments on
653 the basis of ternary diagrams. Cont Shelf Res.
654 https://doi.org/http://dx.doi.org/10.1016/S0278-4343(00)00015-7

655 Fuentes, C., Haverkamp, R., Parlange, J.-Y., 1992. Parameter constraints on closed-form
656 soilwater relationships. J Hydrol 134, 117–142. https://doi.org/10.1016/0022-
657 1694(92)90032-Q

658 Gershenzon, N.I., Ritzi Jr., R.W., Dominic, D.F., Mehnert, E., Okwen, R.T., 2016.
659 Comparison of CO2 trapping in highly heterogeneous reservoirs with Brooks-Corey and
660 van Genuchten type capillary pressure curves. Adv Water Resour 96, 225–236.
661 https://doi.org/10.1016/J.ADVWATRES.2016.07.022

662 Gor, G.Y., Elliot, T.R., Prévost, J.H., 2013. Effects of thermal stresses on caprock integrity
663 during CO2 storage. Int J Greenh Gas Control.
664 https://doi.org/https://doi.org/10.1016/j.ijggc.2012.11.020

665 Ingram, R.L., 1953. Fissility of mudrocks. Geol Soc Am Bull 64, 869–878.

666 Ippisch, O., Vogel, H.-J., Bastian, P., 2006. Validity limits for the van Genuchten–Mualem
667 model and implications for parameter estimation and numerical simulation. Adv Water
668 Resour 29, 1780–1789.
669 https://doi.org/http://dx.doi.org/10.1016/j.advwatres.2005.12.011

Krevor, S.C.M., Pini, R., Zuo, L., Benson, S.M., 2012. Relative permeability and trapping of CO2 and water in sandstone rocks at reservoir conditions. Water Resour Res 48. https://doi.org/10.1029/2011WR010859

Lenhard, R.J., Parker, J.C., Mishra, S., 1989. On the Correspondence between Brooks-Corey and van Genuchten Models. J Irrig Drain Eng 115, 744–751. https://doi.org/10.1061/(ASCE)0733-9437(1989)115:4(744)

Li, B., Tchelepi A., H., Benson M., S., 2013. The influence of capillary entry pressure representation on CO2 solubility trapping. Energy Procedia 37, 3808–3815.

Liu, F., Lu, P., Zhu, C., Xiao, Y., 2011. Coupled reactive flow and transport modeling of CO2 sequestration in the Mt. Simon sandstone formation, Midwest U.S.A. Int J Greenh Gas Control. https://doi.org/https://doi.org/10.1016/j.ijggc.2010.08.008

Macquaker, J.H.S., Adams, A.E., 2003. Maximizing Information from Fine-Grained Sedimentary Rocks: An Inclusive Nomenclature for Mudstones. J Sediment Res 73, 735–744. https://doi.org/10.1306/012203730735

Mathias, S.A., Gluyas, J.G., González Martínez de Miguel, G.J., Bryant, S.L., Wilson, D., 2013. On relative permeability data uncertainty and CO2 injectivity estimation for brine aquifers. Int J Greenh Gas Control 12, 200–212. https://doi.org/10.1016/J.IJGGC.2012.09.017

Middleton, R.S., Keating, G.N., Stauffer, P.H., Jordan, A.B., Viswanathan, H.S., Kang, Q.J., Carey, J.W., Mulkey, M.L., Sullivan, E.J., Chu, S.P., Esposito, R., Meckel, T.A., 2012. The cross-scale science of CO2 capture and storage: from pore scale to regional scale. Energy Environ Sci 5, 7328–7345. https://doi.org/10.1039/C2EE03227A

Morel-Seytoux, H.J., Meyer, P.D., Nachabe, M., Tourna, J., van Genuchten, M.T., Lenhard, R.J., 1996. Parameter Equivalence for the Brooks-Corey and Van Genuchten Soil Characteristics: Preserving the Effective Capillary Drive. Water Resour Res 32, 1251–1258. https://doi.org/10.1029/96WR00069

Okwen, R., Stewart, M., Cunningham, J., 2011. Effect of Well Orientation (Vertical vs. Horizontal) and Well Length on the Injection of CO2 in Deep Saline Aquifers. Transp Porous Media 90, 219–232. https://doi.org/10.1007/s11242-010-9686-5

Onoja, M.U., Shariatipour, S.M., 2018. The impact of gradational contact at the reservoir-seal interface on geological CO2 storage capacity and security. Int J Greenh Gas Control 72, 1–13. https://doi.org/10.1016/J.IJGGC.2018.03.007

Onoja, M.U., Williams, J.D.O., Vosper, H., Shariatipour, S.M., 2019. Effect of sedimentary heterogeneities in the sealing formation on predictive analysis of geological CO2 storage. Int J Greenh Gas Control 82, 229–243. https://doi.org/10.1016/J.IJGGC.2019.01.013

Oostrom, M., White, M.D., Porse, S.L., Krevor, S.C.M., Mathias, S.A., 2016. Comparison of relative permeability–saturation–capillary pressure models for simulation of reservoir CO2 injection. Int J Greenh Gas Control 45, 70–85. https://doi.org/https://doi.org/10.1016/j.ijggc.2015.12.013

Perrin, J.-C., Benson, S., 2010. An Experimental Study on the Influence of Sub-Core Scale Heterogeneities on CO2 Distribution in Reservoir Rocks. Transp Porous Media 82, 93–109. https://doi.org/10.1007/s11242-009-9426-x

713 Picard, M.D., 1971. Classification of fine-grained sedimentary rocks. J Sediment Res 41,
714 179–195. https://doi.org/10.1306/74D7221B-2B21-11D7-8648000102C1865D

715 Potter, P.E., Maynard, J.B., Depetris, P.J., 2005. Mud and Mudstones: Introduction and
716 Overview. Springer-Verlag Berlin Heidelberg, Berlin, Heidelberg.

717 Potter, P.E., Maynard, J.B., Pryor, W.A., 1980. Sedimentology of Shale: Study Guide and
718 Reference Source. Springer-Verlag, New York.

719 Pruess, K., Nordbotten, J., 2011. Numerical Simulation Studies of the Long-term Evolution of
720 a CO2 Plume in a Saline Aquifer with a Sloping Caprock. Transp Porous Media 90,
721 135–151. https://doi.org/10.1007/s11242-011-9729-6

722 Sakaki, T., Plampin, M.R., Pawar, R., Komatsu, M., Illangasekare, T.H., 2013. What controls
723 carbon dioxide gas phase evolution in the subsurface? Experimental observations in a
724 4.5 m-long column under different heterogeneity conditions. Int J Greenh Gas Control
725 17, 66–77. https://doi.org/10.1016/J.IJGGC.2013.03.025

726 Shepard, F.P., 1954. Nomenclature based on sand-silt-clay ratios. J Sediment Res 24, 151–
727 158. https://doi.org/10.1306/D4269774-2B26-11D7-8648000102C1865D

728 Singh, V.P., Cavanagh, A., Hansen, H., Nazarian, B., Iding, M., Ringrose, P.S., 2010.
729 Reservoir Modeling of CO2 Plume Behavior Calibrated Against Monitoring Data From
730 Sleipner, Norway, in: SPE Annual Technical Conference and Exhibition. Society of
731 Petroleum Engineers, Florence, Italy. https://doi.org/10.2118/134891-MS

732 Stow, D.A. V, 1981. Fine-grained sediments: Terminology. Q J Eng Geol Hydrogeol 14,
733 243–244. https://doi.org/10.1144/GSL.QJEG.1981.014.04.02

734 USDA, 1987. Soil Mechanics Level I, Module 3: USDA Textural Soil Classification. United
735 States Department of Agriculture, Soil Conservation Service.

736 Van Genuchten, M.T., 1980. A closed form equation for predicting the hydraulic conductivity
737 of unsaturated soils. Soil Sci Soc Am J 44, 892–898.

738 Vogel, T., Cislerova, M., 1988. On the reliability of unsaturated hydraulic conductivity
739 calculated from the moisture retention curve. Transp Porous Media 3, 1–15.
740 https://doi.org/10.1007/BF00222683

741 Vogel, T., van Genuchten, M.T., Cislerova, M., 2000. Effect of the shape of the soil hydraulic
742 functions near saturation on variably-saturated flow predictions. Adv Water Resour 24,
743 133–144. https://doi.org/10.1016/S0309-1708(00)00037-3

744 Wentworth, C.K., 1922. A Scale of Grade and Class Terms for Clastic Sediments. J Geol 30,
745 377–392. https://doi.org/10.1086/622910

746 Yamamoto, H., Doughty, C., 2011. Investigation of gridding effects for numerical simulations
747 of CO2 geologic sequestration. Int J Greenh Gas Control.
748 https://doi.org/https://doi.org/10.1016/j.ijggc.2011.02.007

749 Yoshida, N., Levine, J.S., Stauffer, P.H., 2016. Investigation of uncertainty in CO2 reservoir
750 models: A sensitivity analysis of relative permeability parameter values. Int J Greenh
751 Gas Control. https://doi.org/http://dx.doi.org/10.1016/j.ijggc.2016.03.008

752 Zhou, Q., Birkholzer, J.T., Mehnert, E., Lin, Y.-F., Zhang, K., 2010. Modeling Basin- and

753 Plume-Scale Processes of CO2 Storage for Full-Scale Deployment. Ground Water 48,
754 494–514. https://doi.org/10.1111/j.1745-6584.2009.00657.x

755 Zhou, Q., Birkholzer, J.T., Tsang, C.-F., Rutqvist, J., 2008. A method for quick assessment
756 of CO2 storage capacity in closed and semi-closed saline formations. Int J Greenh Gas
757 Control. https://doi.org/http://dx.doi.org/10.1016/j.ijggc.2008.02.004